Tales of the Venerable Honolulu Tide Gauge*

JOHN A. COLOSI+

Woods Hole Oceanographic Institution, Woods Hole, Massachusetts

WALTER MUNK

Scripps Institution of Oceanography, La Jolla, California

(Manuscript received 30 July 2003, in final form 20 January 2004)

ABSTRACT

Surface expressions of internal tides constitute a significant component of the total recorded tide. The internal component is strongly modulated by the time-variable density structure, and the resulting perturbation of the recorded tide gives a welcome look at twentieth-century interannual and secular variability. Time series of mean sea level $h_{SL}(t)$ and total recorded M_2 vector $\mathbf{a}_{TT}(t)$ are extracted from the Honolulu 1905–2000 and Hilo 1947–2000 (Hawaii) tide records. Internal tide parameters are derived from the intertidal continuum surrounding the M_2 frequency line and from a Cartesian display of $\mathbf{a}_{TT}(t)$, yielding a_{ST} = 16.6 and 22.1 cm, a_{IT} = 1.8 and 1.0 cm for surface and internal tides at Honolulu and Hilo, respectively. The proposed model $a_{TT}(t) = a_{ST} + a_{IT}\cos\theta_{IT}(t)$ is of a phase-modulated internal tide generated by the surface tide at some remote point and traveling to the tide gauge with velocity modulated by the underlying variable density structure. Mean sea level $h_{SL}(t)$ [a surrogate for the density structure and hence for $\theta_{IT}(t)$] is coherent with $a_{IT}(t)$ within the decadal band 0.2–0.5 cycles per year. For both the decadal band and the century drift the recorded M_2 amplitude is high when sea level is high, according to $\delta\mathbf{a}_{TT} = O(0.1\delta h_{SL})$. The authors attribute the recorded secular increase in the Honolulu M_2 amplitude from a_{TT} = 16.1 to 16.9 cm between 1915 and 2000 to a 28° rotation of the internal tide vector in response to ocean warming.

1. Introduction

The Honolulu, Hawaii, tide record goes back to 1872 (Fig. 1), before the end of the monarchy[1] on 17 January 1893, but good data are available only since 1905[2] (Fig. 2). There are older tide records; a "modern" tide recorder was established at St. Helena (16°S, 6°W) in 1784, with occasional short tide-pole readings going back to 1761 (D. Cartwright 2001, personal communication).

Figure 2 shows the Honolulu and Hilo, Hawaii, M_2 tides from a complex demodulation (more later). Both amplitude and phase exhibit variability on a broad range of frequencies, roughly 10% in amplitude and phase (radians). The variability is much too large to be sensibly accounted for by surface tide (ST) variability, suggesting a significant contribution from a time-variable internal tide (IT), as has been proposed by other authors.

With the advent of electronic computers in the 1960s it became possible to perform high-resolution spectral analyses that revealed a *continuum* between the *discrete* tidal spectral lines (Munk and Bullard 1963; Munk et al. 1965). Analysis of the Honolulu 1905–58 tide record (Munk and Cartwright 1966) revealed an enhancement of the intertidal continuum near the strong tidal lines. The record from 1938 to 1950 is broken into segments of T = 1 month (Fig. 3, left) and T = 1 yr (Fig. 3, right),

[1] We are most grateful to D. Cox, R. Ray, and M. A. Merrifield for having searched the historical record.

[2] We have corrected for an (almost forgotten) half-hour time shift from -10.5^h to -11^h UTC that occurred at all Hawaiian tide gauges on 8 June 1947 (Schmitt and Cox 1992). There appears to be another 30-min time shift around 1910 for which we have found no historical record.

* Woods Hole Oceanographic Institution Contribution Number 10975.

+ Current affiliation: Department of Oceanography, Naval Postgraduate School, Monterey, California.

Corresponding author address: John A. Colosi, Naval Postgraduate School, Dept. of Oceanography, 833 Dyer Rd., Monterey, CA 93943.
E-mail: jacolosi@nps.edu

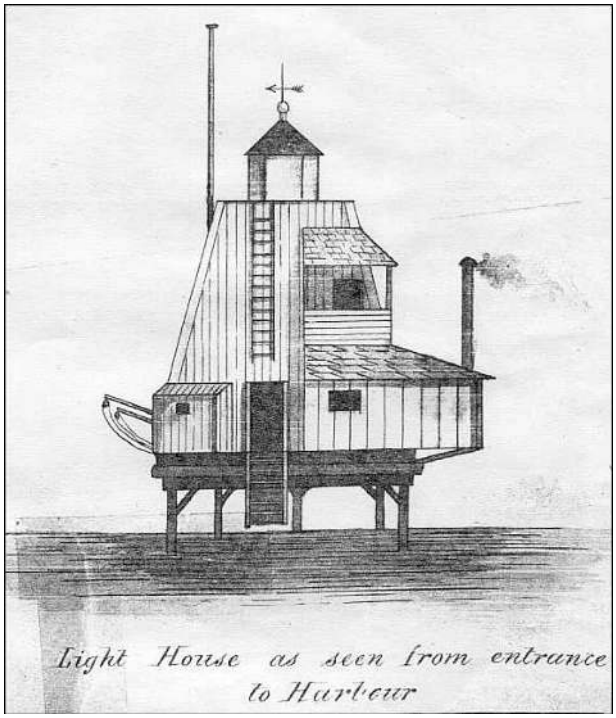

FIG. 1. Sketch by G. E. G. Jackson of the Hawaiian Government Survey (HGS), which was established in 1870 to create a triangulation network on each island to which the individual surveys could be tied. It appears that the HGS was so anxious to establish its sea level datum that it based its "mean" sea level on the half-tide level on a single day (10 Jul 1872). That half-tide level was only 0.02 ft lower than the average half-tide level for 1924–42 and 0.04 ft lower than the relative mean sea level.

respectively. The height of the columns gives the ensemble average of the energy $E_j(T)$ per harmonic j for record length T. The upper panels of Fig. 3 refer to the equilibrium tide $E_j^{\mathrm{ET}}(T)$ numerically generated hour by hour directly from the Kepler–Newton laws and the known orbital constants of moon and sun. To the left, the semidiurnal *species* are split into *groups* at cycles-per-month (cpm) resolution. The spectrum is dominated by the M_2 group [1.93 cycles per day (cpd)]. To the right, the groups are further split into *constituents* at cycles per year (cpy) resolution. Within the M_2 group the constituent at exactly 2 cycles per lunar day strongly dominates. This gives the equilibrium spectrum a cusp-like appearance.

The lower panels of Fig. 3 differentiate between the energies of the Honolulu record that are coherent (black) and incoherent (white) with the equilibrium tide. Write

$$E_j(T) = E^{\mathrm{LINE}}\delta(j) + E_J^{\mathrm{BAND}}(T) \tag{1}$$

for the coherent (line) and incoherent (band) contributions to harmonic j of record length T (Fig. 4), arbitrarily taking the origin of j at the harmonic centered on M_2 with $j = \pm 1, \pm 2, \ldots$ designating neighboring harmonics at intervals of $\Delta f = T^{-1}$. For the specific case of the harmonic $j = 0$,

$$E_0(T) = E^{\mathrm{LINE}} + E_0^{\mathrm{BAND}}(T). \tag{2}$$

In both Eqs. (1) and (2) the line energy contains a mix of ST and IT contributions; the band is associated with only the IT. Write

$$E^{\mathrm{BAND}} \equiv \sum_{j=-\infty}^{\infty} E_j^{\mathrm{BAND}} \tag{3}$$

for the *total* band energy (including $j = 0$); E^{BAND} is independent of T, so E_j^{BAND} is proportional to $1/T$: shorter records have fewer harmonics of larger amplitude, and E_0^{BAND} contains a relatively large fraction of E^{BAND}. At low (cpm) resolution, most of the band energy has been absorbed in the central harmonic. However, E^{LINE} is not a function of T. We shall take advantage of these properties in our attempt to separate the barotropic (surface) and baroclinic (internal) tide components.

Each constituent is associated with a line and a band. Energetic constituents have large lines and large bands. At cpm resolution, the incoherent energy is peaked at M_2 (Fig. 3, third panel) because M_2 is the dominant constituent (not because of any inherent property of the shape of the band spectrum, as we will show). It was this peaked appearance that led Munk and Cartwright (1966) to refer to tidal "cusps," an unfortunate term for the gentle rise associated with the incoherent band at adequate resolution (Fig. 3, right). The distinction between the sharp M_2 peak in the equilibrium spectrum and the broad rise in the sidebands is but a manifestation of the sharp frequency discrimination of orbital mechanics as compared with the broad resonances encountered in ocean dynamics. In all further discussion we shall use the traditional designations of spectral *lines* and *bands.*

Munk and Cartwright associated the tidal bands to low-frequency modulations but did not make any connections with internal tides; they referred to a personal communication by T. Sakou and G. Groves (1966), suggesting that "the cusp (band) energy represents the small surface oscillations associated with internal tides. The spreading into cusps is to be associated with a modulation of the internal tides by the slowly varying thermal structure." Munk et al. (1965) remarked that, "it is amusing to contemplate that a record of climatic fluctuations is contained in the cusps and could in prin-

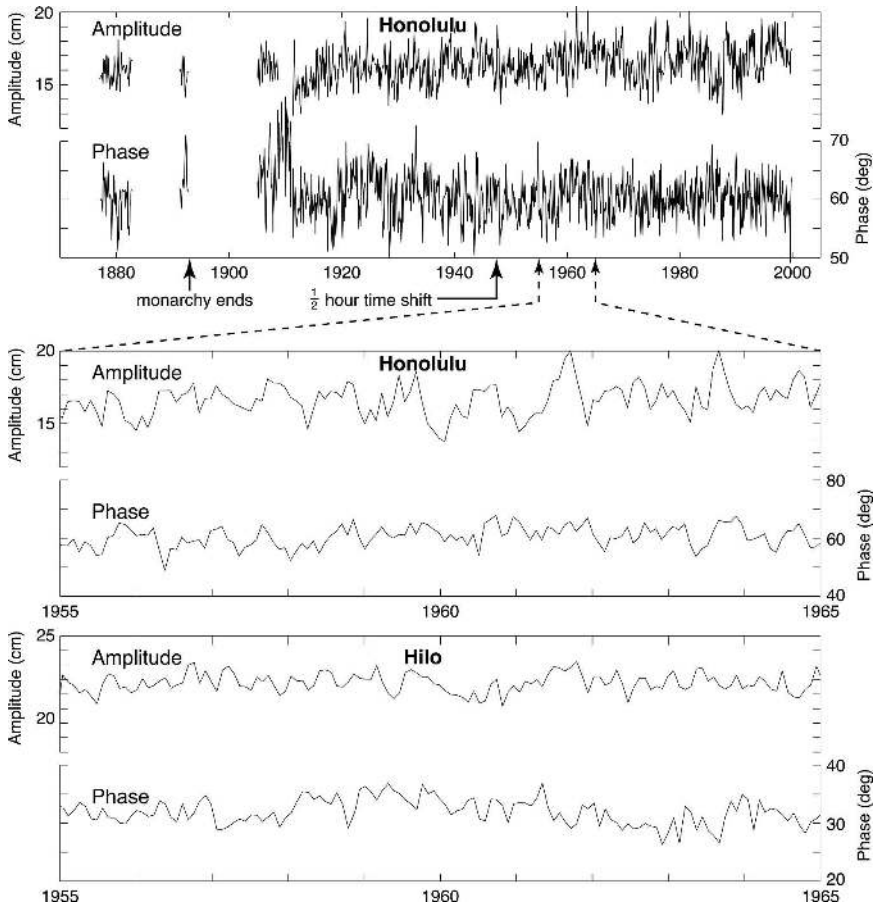

FIG. 2. The M_2 amplitude and phase *lag* (Greenwich epoch) of the Honolulu and Hilo tide records from a complex demodulation using the gravitational tide potential.

ciple be recovered by demodulation at tidal frequencies. Thus one could study the low-frequency fluctuations even if the recording instruments do not have the prerequisite long-term stability."

There the matter rested for 30 years, until Ray and Mitchum (1997) attacked the problem of disentangling the ST and IT contributions to E_0. They found that M_2 amplitudes measured at the offshore site of the Hawaii Ocean Time-Series (HOT) 1991–94 with inverted echo sounders could be correlated with amplitudes measured by coastal tide gauges along the north side of the Hawaiian Ridge. Further, Mitchum and Chiswell (2000) demonstrated that the large M_2 amplitudes occurred at times of a relatively deep thermocline (high sea level). The authors envision a barotropic–baroclinic mode conversion at a nearby shelf break and modulated by the variable depth of the thermocline. Guided by the numerical simulations of Alford et al. (2006), we envision a dominant source area of surface-to-internal mode conversion near Makapuu Point, well separated from the recording site in Mamala Bay (Fig. 5), with changes in the density structure causing changes in the internal phase speed and accordingly modulating the internal tide phase.[3]

The detection by satellite altimetry (Ray and Mitchum 1996) and by acoustic tomography (Dushaw et al. 1995) of internal tides emanating from the Hawaiian Island ridge constitute benchmarks in any further development of the subject [see review by Ray and Mitchum (1997)]. Ray and Cartwright (2001) combined the altimetry data with climatological hydrographic data to deduce the flux of IT energy. The baroclinic component of E_0^{LINE} is extracted on the basis of IT wavelengths: 150 and 85 km for modes 1 and 2, as compared with order 10 000 km for the surface mode.[4]

[3] There is some resemblance to the phase-variable internal tides on the New England shelf resulting from modulation by the meandering shelfbreak front and by slope eddies (Colosi et al. 2001).

[4] There is no measurable band energy in the offshore record (R. Ray 2002, personal communication).

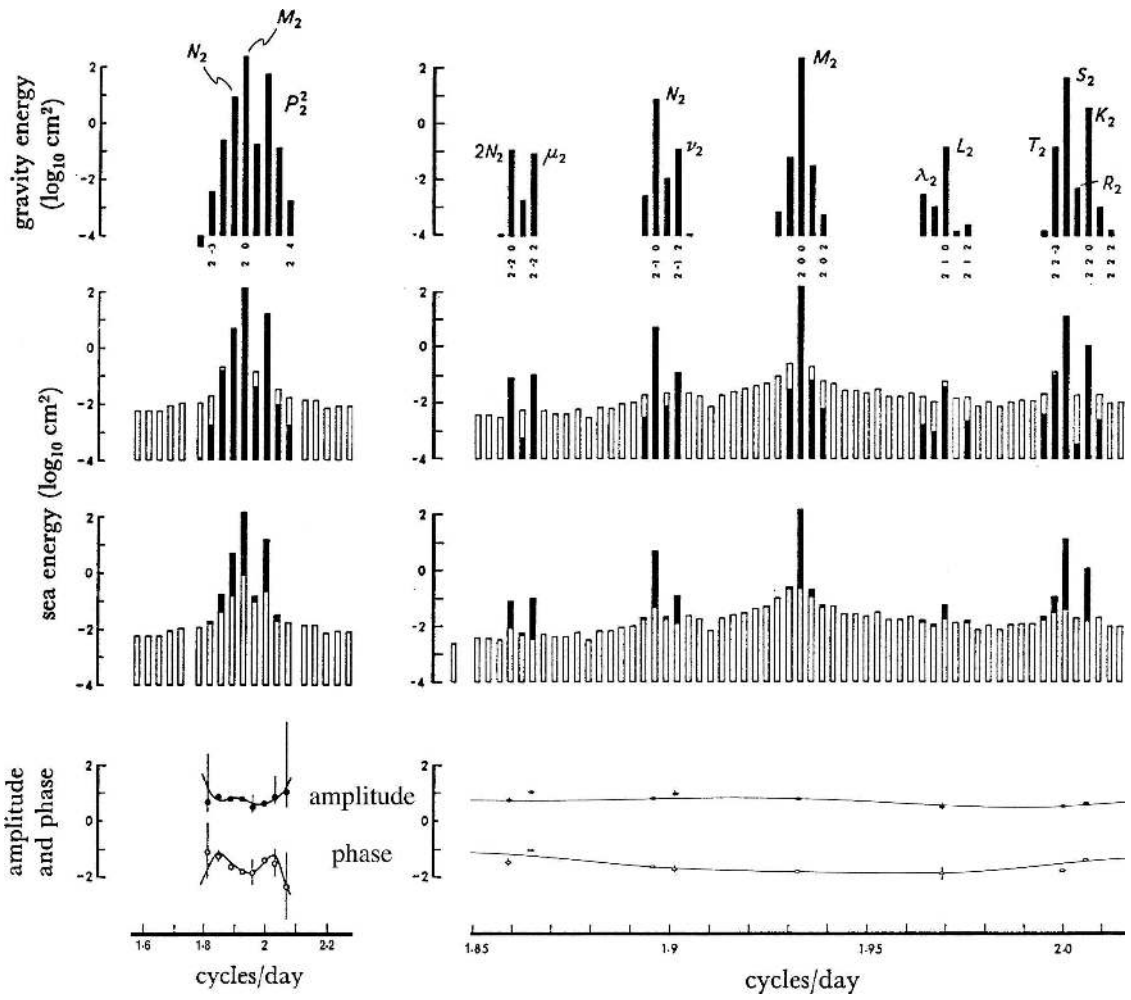

FIG. 3. Honolulu semidiurnal tide spectra at (left) cpm and (right) cpy resolution (from Munk and Cartwright 1966). The top panels show the energy per harmonic of the equilibrium tide relative to 10^{-4} cm^2. In the next two panels, the observed spectrum is designated by the total heights of the columns, with the height of the filled portions designating energy coherent with the equilibrium tide and the unfilled portion designating noncoherent energy. Bottom panels give amplitude and phase *lead* (!) relative to the local equilibrium tide.

Analysis of a single tide gauge record does not offer this opportunity for spatial discrimination.

In the following sections we attempt a separation of the barotropic and baroclinic components from a single tide record. A toy model with parameters close to those found in the subsequent Honolulu record analysis is used for guidance and validation (see first row of Table 1).

2. Internal tide modulation in the frequency domain

The combined surface plus internal tidal elevation is written

$$h(t) = a_{\mathrm{ST}} e^{i(2\pi f_c t - \theta_{\mathrm{ST}})} + [a_{\mathrm{IT}} + \delta a(t)] e^{i[2\pi f_c t - \theta_{\mathrm{IT}} - \theta(t)]}, \tag{4}$$

where f_c is the "carrier" frequency associated with the M_2 tide (or any other constituent) and $\theta(t)$ is departure from the mean phase θ_{IT}, with variance $\overline{\theta^2}$. The instantaneous frequency $f_c + d\theta/dt$ spills the IT energy into the neighboring harmonics. The important parameter

$$\nu^2 \equiv e^{-\overline{\theta^2}} \tag{5}$$

has a simple interpretation for long records of internal tides only. The energy in the j'th harmonic is

$$E_j = E_{\mathrm{IT}}^{\mathrm{LINE}} \delta_j + E_j^{\mathrm{BAND}}, \quad E^{\mathrm{BAND}} = \sum_{j=-\infty}^{\infty} E_j^{\mathrm{BAND}},$$

$$E_{\mathrm{IT}}^{\mathrm{LINE}} = \frac{1}{2} a_{\mathrm{IT}}^2 \nu^2, \quad \text{and} \quad E^{\mathrm{BAND}} = \frac{1}{2} a_{\mathrm{IT}}^2 (1 - \nu^2), \tag{6}$$

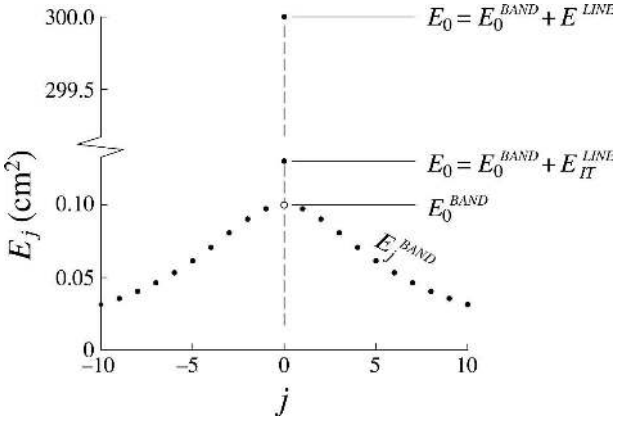

FIG. 4. Cartoon of total (surface plus internal) tide spectrum with a phase-modulated IT component. Filled dots give total energy E_j of harmonic j at frequency $\Delta f = jT^{-1}$ relative to the M_2 tidal frequency, where T is record length; E_j^{BAND} is the spectral continuum associated with the internal tide. For the case of internal tides only, the measured energy at the carrier (tidal) frequency $j = 0$ is $E_0 = E_0^{\mathrm{BAND}} + E_{\mathrm{IT}}^{\mathrm{LINE}}$, where E_0^{BAND} (open dot) is inferred from neighboring band harmonics and $E_{\mathrm{IT}}^{\mathrm{LINE}}$ is the line spectrum of the internal tide. In the general case of surface plus internal tides, $E_0 = E_0^{\mathrm{BAND}} + E^{\mathrm{LINE}}$, where E^{LINE} is the magnitude of the vector sum of surface plus internal tide energies.

where $f_j = f_c + jT^{-1}$ is the frequency of the j'th harmonic for a record of length T. The issue of $\delta a(t) \neq 0$ is taken up in section 2d.

a. Lorentzian phase modulation

The spectrum E_j depends on the details of the $\theta(t)$ modulation. For the special case that $\theta(t)$ is a Gaussian random variable with a Lorentzian spectrum

$$S_\theta(f) = \pi^{-1}\overline{\theta^2}\,\frac{f_\theta}{f_\theta^2 + f^2}, \quad \int_{-\infty}^{\infty} df\, S_\theta(f) = \overline{\theta^2}, \tag{7}$$

E_j has a simple analytical solution. For $a_{\mathrm{ST}} = 0$,

$$h(t) = a_{\mathrm{IT}} e^{i[2\pi f_c t - \theta_{\mathrm{IT}} - \theta(t)]} \tag{8}$$

with a Fourier transform

$$\begin{aligned} H(f) &= \frac{1}{\sqrt{2}T}\int_{-T/2}^{T/2} dt\, h(t) e^{-2\pi i f t} \\ &= \frac{e^{-i\theta_{\mathrm{IT}}}}{\sqrt{2}T}\int_{-T/2}^{T/2} dt\, a_{\mathrm{IT}} e^{-2\pi i(f - f_c)t} e^{-i\theta(t)} \end{aligned} \tag{9}$$

(the rationale for the normalization will become clear later). For θ a zero-mean Gaussian random variable,

$$\langle \exp[-i\theta(t)]\rangle = \exp(-\overline{\theta^2}/2) = \nu, \tag{10}$$

yielding an expected value

$$\langle H(f)\rangle = a_{\mathrm{IT}}\nu\sqrt{\frac{1}{2}}\,\mathrm{sinc}(f - f_c)T; \quad \mathrm{sinc}\, x \equiv \sin\pi x/\pi x. \tag{11}$$

The mean phase angle is determined by

$$\tan\theta_{\mathrm{IT}} = \frac{\Im\langle H\rangle}{\Re\langle H\rangle}. \tag{12}$$

The expected value of the power spectrum of the phase-modulated internal tide is given by

$$\langle HH^*\rangle = \frac{a_{\mathrm{IT}}^2}{2T^2}\int\int_{-T/2}^{T/2} dt_1\, dt_2\, e^{-2\pi i(f - f_c)\Delta t} e^{-D(|\Delta t|)/2}, \tag{13}$$

where $\Delta t = t_1 - t_2$,

$$D[|\Delta(t)|] \equiv \langle[\theta(t_1) - \theta(t_2)]^2\rangle = 2\overline{\theta^2}(1 - e^{-2\pi f_\theta|\Delta t|}), \tag{14}$$

f_θ is the characteristic frequency of the phase modulation, D is the phase structure function for the spectrum [Eq. (6)], and

$$\begin{aligned} e^{-(1/2)D} &= \nu^2 \exp(\overline{\theta^2} e^{-2\pi f_\theta|\Delta t|}) \\ &= \nu^2\left[1 + \sum_{n=1}^{\infty}\frac{(\overline{\theta^2})^n}{n!} e^{-2\pi n f_\theta|\Delta t|}\right]. \end{aligned} \tag{15}$$

The double integral in Eq. (13) can be evaluated analytically (appendix B). Details are cumbersome and uninteresting. The result is

$$\begin{aligned} \langle HH^*\rangle &= \frac{1}{2} a_{\mathrm{IT}}^2\nu^2[\mathrm{sinc}^2(f - f_c)T + \tau^{-1}G(\overline{\theta^2}, \beta, \tau)], \\ \beta &= (f - f_c)/f_\theta, \quad \text{and} \quad \tau \equiv 2\pi f_\theta T, \end{aligned} \tag{16}$$

where G is given in appendix A. The band spectrum component of this spectrum is given by

$$E_j^{\mathrm{BAND}} = \frac{1}{2} a_{\mathrm{IT}}^2\nu^2\tau^{-1}G_j(\overline{\theta^2}, \beta, \tau). \tag{17}$$

b. Long records

In the limit of large τ,

$$\mathrm{sinc}^2[(f - f_c)T] \to \frac{\delta(f - f_c)}{T} = \frac{\delta(\beta)}{Tf_\theta}, \tag{18}$$

$$\langle HH^*\rangle = \frac{1}{2} a_{\mathrm{IT}}^2\nu^2\tau^{-1}[2\pi\delta(\beta) + F(\overline{\theta^2}, \beta)], \tag{19}$$

with F defined in appendix A. We shall identify

$$T\langle HH^*\rangle \equiv S_h(f) = \frac{1}{2} a_{\mathrm{IT}}^2\nu^2\,\frac{1}{2\pi f_\theta}[2\pi\delta(\beta) + F(\overline{\theta^2}, \beta)] \tag{20}$$

with the power spectral *density*; for a_{IT} in centimeters

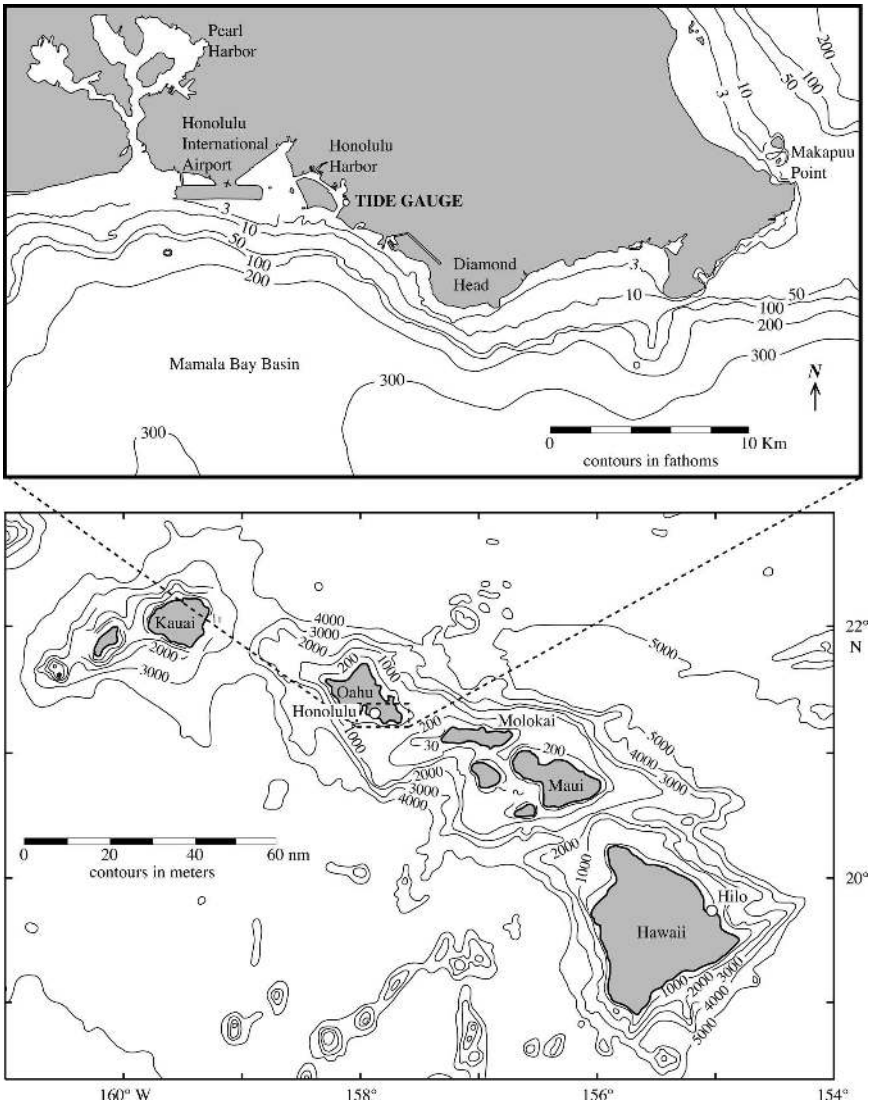

FIG. 5. Chart showing Makapuu Point, Mamala Bay, and the Honolulu tide gauge. Calculations by M. A. Merrifield and P. Holloway (2002, personal communication) indicate an internal tide propagating westward from a generation area near Makapuu Point.

and f_θ in cycles per day, $S_h(f)$ is in square centimeters per cycle per day.

The "long record" approximation [Eq. (19)] is well known in the communication literature (e.g., Middleton 1960, p. 606]. It consists of a spectral line at $\beta = 0$, hence $f = f_c$ (the "line"), plus a surrounding continuum (the "band"). Using $df = f_\theta\, d\beta$, we have

$$\int_{-\infty}^{\infty} df\, S_h(f) = \frac{1}{2} a_{\mathrm{IT}}^2 \nu^2 \left[1 \; \frac{1}{\pi} \sum_{n=1}^{\infty} \frac{(\overline{\theta^2})^n}{(n-1)!} \frac{2}{n} \int_0^{\infty} \frac{n\, d\beta}{\beta^2 + n^2} \right]. \tag{21}$$

The integral equals $\pi/2$, and the bracket becomes

$$[\,] = 1 + \sum_{1}^{\infty} \frac{(\overline{\theta^2})^n}{n!} = 1 + \sum_{0}^{\infty} \frac{(\overline{\theta^2})^n}{n!} - 1 = e^{+\overline{\theta^2}} = \nu^{-2}. \tag{22}$$

Thus,

$$\int_{-\infty}^{\infty} df\, S_h(f) = \frac{1}{2} a_{\mathrm{IT}}^2 \equiv E_{\mathrm{IT}} = E_{\mathrm{IT}}^{\mathrm{LINE}} + E^{\mathrm{BAND}} \tag{23}$$

with

TABLE 1. The toy model serves as control for the subsequent estimates for Honolulu and Hilo. Separate estimates are made in the frequency domain and in the (Cartesian) time domain. The six assumed toy values (which resemble the Honolulu situation) yield auxiliary parameters (right columns) for estimating the toy values. The frequency analysis yields estimates for three of the six model values (row a); the Cartesian analysis yields five estimates (rows b and c). For the Hilo frequency domain analysis, energy within a frequency range of $\delta f = \pm 1/1240$ day of the M_2 constituent is ignored. All estimates for θ_{IT} are subject to error bars of order rms (θ_{IT}). For the Honolulu and Hilo frequency analysis, estimates of surface tide amplitude and phase are done in the "traditional" fashion with error limits established using Eqs. (33) and (35). Incl is inclination.

		Surface tide		Internal tide				Auxiliary parameters		
		a_{ST} (cm)	θ_{ST} (°)	a_{IT} (cm)	θ_{IT} (°)	rms(θ_{IT}) (°)	f_θ (cpy)	E^{BAND} (cm^2)	E_0^{BAND} (cm^2)	Incl
					Toy model 85-yr equivalent					
	Assumed	17	60	2	310	107	0.5	1.940	0.130	−0.0201
		Frequency domain						E^{BAND}	E_0^{BAND}	Incl
(a)				2.03		97	0.584	1.928	0.131	−0.0202
		Cartesian domain						A	B	
(b)	Uncorrected	$17.0^{+0.4}_{-0.5}$	$59.1^{+1.1}_{-1.3}$	$1.68^{+0.16}_{-0.10}$	287	98^{+11}_{-11}	0.475	1.33 ± 0.12	−0.043 ± 0.11	
(c)	Corrected	$17.0^{+0.4}_{-0.5}$	$59.1^{+1.1}_{-1.3}$	$1.89^{+0.16}_{-0.10}$	287	103^{+11}_{-11}	0.475	1.71 ± 0.12	−0.043 ± 0.11	
(d)	f_L = 3.34 cpy	$17.0^{+0.4}_{-0.5}$	$60.0^{+1.6}_{-1.4}$	$1.89^{+0.20}_{-0.09}$	309	102^{+1}_{-26}		1.71 ± 0.16	−0.070 ± 0.16	
					Honolulu 1915–2000					
		Frequency domain						E^{BAND}	E_0^{BAND}	Incl
(a)		$16.4^{+0.3}_{-0.3}$	$60.4^{+1.0}_{-1.0}$	1.90		112°	0.804	1.77	0.082	−0.0317
		Cartesian domain						A	B	
(b)	Uncorrected	$16.6^{+0.2}_{-0.3}$	$60.2^{+2.9}_{-2.6}$	$1.50^{+0.32}_{-0.00}$	229	119^{+3}_{-48}	0.745	1.23 ± 0.12	−0.1089 ± 0.12	
(c)	Corrected	$16.6^{+0.2}_{-0.3}$	$60.2^{+2.9}_{-2.6}$	$1.79^{+0.36}_{-0.00}$	229	128^{+3}_{-48}	0.745	1.58 ± 0.15		
					Hilo 1947–2000					
		Frequency domain						E^{BAND}	E_0^{BAND}	Incl
(a)		$21.8^{+0.2}_{-0.2}$	$31.1^{+0.4}_{-0.4}$	1.15		116	0.858	0.65	0.022	−0.0133
		Cartesian domain						A	B	
(b)	Uncorrected	$22.1^{+0.7}_{-0.7}$	$31.3^{+0.6}_{-0.6}$	$1.02^{+0.31}_{-0.00}$	233	102^{+4}_{-43}	0.605	0.58 ± 0.07	−0.095 ± 0.07	
(c)	Corrected	$22.1^{+0.7}_{-0.7}$	$31.3^{+0.6}_{-0.6}$	$1.24^{+0.35}_{-0.00}$	233	108^{+4}_{-43}	0.605	0.75 ± 0.09	−0.095 ± 0.07	

$$E_{IT}^{LINE} = \frac{1}{2} a_{IT}^2 \nu^2 \quad \text{and}$$

$$E^{BAND} = \frac{1}{2} a_{IT}^2 (1 - \nu^2) = \sum_{j=-\infty}^{\infty} E_j^{BAND} \tag{24}$$

designating the line and *total* band contributions to the internal tide energy. Further,

$$E_j^{BAND} = \frac{1}{2} a_{IT}^2 \nu^2 \tau^{-1} F_j(\overline{\theta^2}) \tag{25}$$

for the spectrum in centimeters squared per record harmonic. From Eq. (A10), $\Sigma_{j=-\infty}^{\infty} F_j = \tau(\nu^{-2} - 1)$, yielding the previous expression for E^{BAND}. For the special case $j = 0$,

$$E_0 = E_{IT}^{LINE} + E_0^{BAND} = \frac{1}{2} a_{IT}^2 \nu^2 [1 + F_0(\overline{\theta^2})], \tag{26}$$

which has a maximum of $1.0347(\frac{1}{2} a_{IT}^2)$ for $\overline{\theta^2} = 1.50$.

c. Parameter estimates for a toy model

Toy model parameters are chosen that are close to the subsequent M_2 and N_2 estimates for Honolulu (see Table 1, first row, for M_2 values). To allow for interference from the neigboring N_2 constituent, we select

$$a_{ST} = 4.0 \text{ cm}, \quad \theta_{ST} = 45°, \quad a_{IT} = 0.5 \text{ cm},$$
$$\theta_{IT} = -70°, \quad \text{rms } \theta = 107°, \quad \text{and} \quad f_\theta = 0.5 \text{ cpy}.$$

The record length T was chosen to give exactly 2396 M_2 cycles ($T \sim 3.395$ tropical years) and also to give nearly exactly an integer number of N_2 cycles. The phase $\theta(t)$ was generated from a sample of Gaussian random numbers shaped according to the Lorentzian spectrum. Sixteen realizations were generated with four samples per M_2 period over the 1239.99 days. For each realization, spectra $H(f)H^*(f)$ of the real component

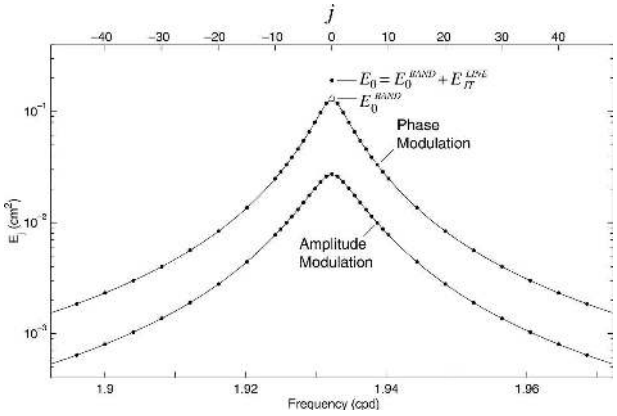

FIG. 6. Spectrum E_j of the toy model (Table 1) with internal tides only. The contribution for phase modulation exceeds that associated with amplitude modulation ($\epsilon = 0.5$; see appendix C).

of $h(t)$ were computed. The ensemble spectrum $\langle HH^* \rangle$ yields $E_0 = 0.180$ cm^2 (Fig. 6).

An initial value of $E_0^{\rm BAND}$ is obtained by extrapolating $j = 0$ energy from the neighboring harmonics $j = \pm 1, \pm 2, \ldots$, and a first estimate of the total band energy is made by summing over as many harmonics as possible, including $E_0^{\rm BAND}$, but avoiding interference with the neighboring constituents. Improved estimates of $E_0^{\rm BAND}$ and $E^{\rm BAND}$ are made by a least squares fit of the noninterfering *normalized* band energies

$$\mathcal{E}_j^{\rm BAND}(\overline{\theta^2}, f_\theta) = \frac{E_j^{\rm BAND}(a_{IT}, \overline{\theta^2}, f_\theta)}{E_0^{\rm BAND}(a_{IT}, \overline{\theta^2}, f_\theta)} = \frac{G_j(\overline{\theta^2}, f_\theta)}{G_0(\overline{\theta^2}, f_\theta)} \tag{27}$$

to the model equations, thus extrapolating $E^{\rm BAND}$ into and beyond the N_2 and L_2 bands (Fig. 3). A search through f_θ ν space leads to satisfactory new estimates of $E^{\rm BAND} = 1.928$ cm^2 and $E_0^{\rm BAND} = 0.131$ cm^2. Thus, $E_{\rm IT}^{\rm LINE} = E_0 - E_0^{\rm BAND} = 0.180 - 0.131 = 0.049$ cm^2.

In summary, the measured spectra yield three auxiliary measured parameters:

$$E_0^{\rm BAND} = 0.131 \text{ cm}^2, \quad E^{\rm BAND} = 1.928 \text{ cm}^2, \quad \text{and} \quad E_{\rm IT}^{\rm LINE} = 0.049 \text{ cm}^2. \tag{28}$$

Using the three relations

$$\frac{E_{\rm IT}^{\rm LINE}}{E^{\rm BAND}} = \frac{\nu^2}{1-\nu^2}, \quad \frac{1}{2}a_{\rm IT}^2 = \frac{E^{\rm BAND}}{1-\nu^2}, \quad \text{and}$$

$$\tau = 2\pi f_\theta T \rightarrow E_0^{\rm BAND} = E_{\rm IT}^{\rm LINE}\frac{G_0(\overline{\theta^2}, f_\theta)}{\tau} \tag{29}$$

yields the estimated M_2 values

$$a_{\rm IT} = 1.99 \text{ cm}, \quad \text{rms } \theta = 110°, \quad \text{and} \quad f_\theta = 0.49 \text{ cpy}, \tag{30}$$

which compare favorably to the "true" M_2 values 2 cm, 107°, and 0.50 cpy.

d. Amplitude modulation

The contribution of amplitude modulation to the internal tide [Eq. (4) with $a_{\rm ST} = 0$] is considered in appendix C. For the case of Lorentzian spectra for both amplitude and phase modulation, the internal tide spectrum consists of two components, one due solely to the previously derived phase modulation and one that has a mixture of phase and amplitude modulation effects [Eq. (C9)]. The amplitude modulation makes no contribution to $E^{\rm LINE}$; for the case $\epsilon^2 = \langle \delta a_{\rm IT}^2 \rangle / a_{\rm IT}^2 = 0.25$ (Fig. 6), the phase contribution clearly dominates, primarily from the requirement that $\epsilon \ll 1$, a consequence of amplitude being a positive definite quantity. In the following treatment, amplitude modulation is ignored.[5] Observations (section 5c) support a dominant role of phase modulation.

3. Combined surface and internal tides

The combined surface and internal tide record

$$h(t) = a_{\rm ST}e^{i(2\pi f_c t - \theta_{\rm ST})} + a_{\rm IT}e^{i[2\pi f_c t - \theta_{\rm IT} - \theta(t)]} \tag{31}$$

has a spectrum

$$\langle H(f) \rangle = \sqrt{\frac{1}{2}}\,\text{sinc}[(f - f_c)T](a_{\rm ST}e^{-i\theta_{\rm ST}} + a_{\rm IT}\nu e^{-i\theta_{\rm IT}}) \tag{32}$$

in place of Eq. (11), with phase angle

$$\tan\psi = \frac{\Im\langle H \rangle}{\Re\langle H \rangle} = -\frac{a_{\rm ST}\sin\theta_{\rm ST} + a_{\rm IT}\nu\sin\theta_{\rm IT}}{a_{\rm ST}\cos\theta_{\rm ST} + a_{\rm IT}\nu\cos\theta_{\rm IT}}. \tag{33}$$

The power spectrum is

$$\langle HH^* \rangle = \text{sinc}^2[(f - f_c)T]\left[\frac{1}{2}a_{\rm ST}^2 + \frac{1}{2}a_{\rm IT}^2\nu^2 + a_{\rm ST}a_{\rm IT}\nu\cos(\theta_{\rm IT} - \theta_{\rm ST})\right] + \frac{1}{2}a_{\rm IT}^2\nu^2\tau^{-1}G. \tag{34}$$

Here $E^{\rm BAND}$ and $E_j^{\rm BAND}$ are given by the previous Eqs. (6) and (17);

[5] The reviewer called our attention to the analysis of internal tides by Chiswell (2002) at the offshore station ALOHA north of Oahu. Here the record is dominated by an amplitude modulation attributed to the orbital currents associated with Rossby waves.

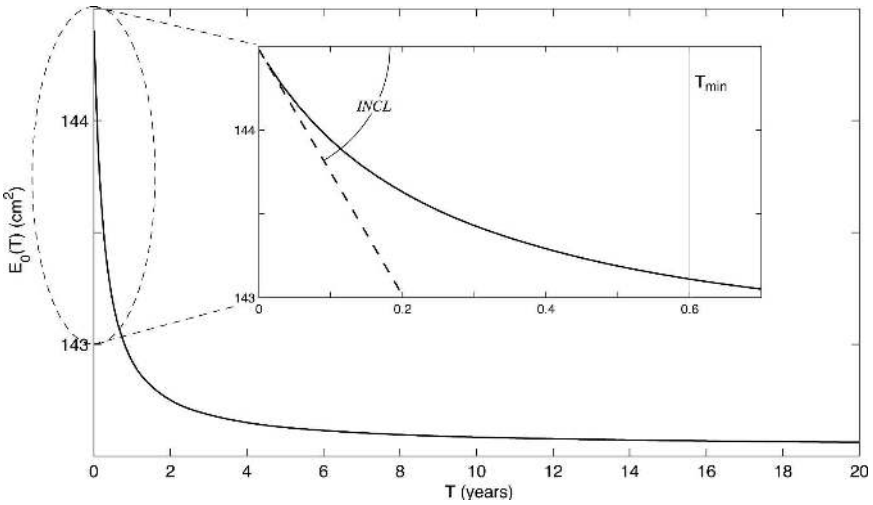

FIG. 7. The line energy $E_0(T)$ as a function of record length T for the toy model. Here E^{BAND} can be inferred from the difference at large and small T. The inset gives an expanded view for small T. The analysis is limited to $T > T_{\mathrm{min}}$ by interference from the neighboring N_2 constituent.

$$E^{\mathrm{LINE}} = \frac{1}{2}a_{\mathrm{ST}}^2 + \frac{1}{2}a_{\mathrm{IT}}^2\nu^2 + a_{\mathrm{ST}}a_{\mathrm{IT}}\nu\cos(\theta_{\mathrm{IT}} - \theta_{\mathrm{ST}}) \tag{35}$$

can be interpreted as interference between vectors $\mathbf{a}_{\mathrm{ST}}$ and $\nu\,\mathbf{a}_{\mathrm{IT}}$ with

$$E^{\mathrm{LINE}} = \frac{1}{2}|\mathbf{a}_{\mathrm{ST}} + \nu\,\mathbf{a}_{\mathrm{IT}}|^2. \tag{36}$$

Previously the three measured parameters E^{LINE}, E^{BAND}, and E_0^{BAND} led to an unambiguous evaluation of a_{IT}, rms θ, f_θ, and the identification ψ with θ_{IT}. We now face the two additional unknowns, a_{ST} and θ_{ST}, and have lost the unique association of ψ with θ_{IT}.

a. Record length

One additional constraint is gained by the dependence of $E_0^{\mathrm{BAND}}(T)$, and hence $E_0(T)$, on record length. Accordingly,

$$E_0(\tau) = E^{\mathrm{LINE}} + \frac{1}{2}a_{\mathrm{IT}}^2\nu^2\tau^{-1}G_0(\overline{\theta^2}, \tau), \tag{37}$$

$$E_0(\infty) = E^{\mathrm{LINE}} = \frac{1}{2}a_{\mathrm{ST}}^2 + \frac{1}{2}a_{\mathrm{IT}}^2\nu^2 + a_{\mathrm{ST}}a_{\mathrm{IT}}\nu\cos(\theta_{\mathrm{IT}} - \theta_{\mathrm{ST}}), \tag{38}$$

and

$$E_0(\tau \to 0) = \frac{1}{2}a_{\mathrm{ST}}^2 + \frac{1}{2}a_{\mathrm{IT}}^2\left(1 + \frac{2}{3}\tau\ln\nu\right) + a_{\mathrm{ST}}a_{\mathrm{IT}}\nu\cos(\theta_{\mathrm{IT}} - \theta_{\mathrm{ST}}) \tag{39}$$

with an inclination near $\tau = 0$ of

$$E_0' \equiv dE_0/d\tau = \frac{1}{3}a_{\mathrm{IT}}^2\ln\nu, \tag{40}$$

in agreement with the model calculation (Fig. 7). The difference

$$E_0(0) - E_0(\infty) = \frac{1}{2}a_{\mathrm{IT}}^2(1 - \nu^2) = E^{\mathrm{BAND}} \tag{41}$$

is another way of determining band energy. The figure is drawn for an arbitrary choice of $\Delta\theta = \theta_{\mathrm{IT}} - \theta_{\mathrm{ST}} = 30°$. For different $\Delta\theta$ the entire curve is translated vertically with no change in shape. There is no information concerning $\Delta\theta$.

b. Parameter estimates for a toy model

For a surface plus internal tide record using the assumed M_2 and N_2 parameters (section 2c and Table 1, row a), three (out of six) M_2 values, a_{IT}, rms θ, and $f\theta$, can be estimated from the three observed parameters

$$E^{\mathrm{BAND}} = 1.928\ \mathrm{cm}^2,$$
$$\mathrm{Incl} \equiv (dE_0/dT)_{T=0} = -0.0202\ \mathrm{cm}^2\ (\mathrm{day})^{-1}, \quad \text{and}$$
$$TE_0^{\mathrm{BAND}}(T) = 1239.99 \times 0.131 = 162\ \mathrm{cm}^2\ (\mathrm{cpd})^{-1}, \tag{42}$$

using the three equations

$$E^{\mathrm{BAND}} = \frac{1}{2} a_{\mathrm{IT}}^2 (1 - \nu^2),$$

$$\mathrm{Incl} = (dE_0/dT)_{\tau=0} = (d\tau/dT)E_0' = \frac{1}{3} a_{\mathrm{IT}}^2 \ln\nu 2\pi f_\theta, \quad \text{and}$$

$$E_0^{\mathrm{BAND}}(T) = \frac{1}{2} a_{\mathrm{IT}}^2 \nu^2 \tau^{-1} G_0(\overline{\theta^2}, \tau). \tag{43}$$

Because of interference from other semidiurnal consituents (most notably N_2 and L_2), the inclination (Incl) cannot be directly estimated in the small T limit. Instead, Incl is inferred by fitting the curve $E_0^{\mathrm{BAND}}(T)$ over several T values. The adopted procedure is to compute spectra at several T values and fit band spectra, as described in section 3c, to give estimates of $E_0^{\mathrm{BAND}}(T)$ and E^{BAND}. The T values are chosen to be an integer number of cycles of the M_2 and nearly an integer number of cycles of the N_2. For a minimum record length of $T = 220.4657$ days the M_2 and N_2 constituents can be separated, and there are an adequate number of points to fit a band spectrum. Fifteen more T values are chosen up to a maximum value of $T = 3857.6317$ days.

The ratio of the first two observables determines a function $f_\theta(\nu)$:

$$2\pi f_\theta = \frac{3}{2} \frac{1 - \nu^2}{\ln\nu} \frac{\mathrm{Incl}}{E^{\mathrm{BAND}}}; \tag{44}$$

multiplying both sides by T yields $\tau(\nu, T)$. All three observables can be combined into the dimensionless observable

$$L(T) = \frac{\mathrm{Incl} \times T \times E_0^{\mathrm{BAND}}(T)}{(E^{\mathrm{BAND}})^2}. \tag{45}$$

Substituting Eq. (43) into Eq. (45) yields

$$L(T) = \phi(\nu, T) \equiv \frac{\frac{2}{3} \nu^2 \ln\nu G_0[-2\ln\nu, \tau(\nu, T)]}{(1 - \nu^2)^2}. \tag{46}$$

A numerical solution of Eq. (46) determines ν, and subsequently f_θ from Eq. (44) and a_{IT} from Eq. (41). Numerical values in Eq. (42) yield $L(T = 1239.99) = -0.860$. A plot of $\phi(\nu, T)$ surprisingly yields two intersections (Fig. 8) corresponding to

$$\nu_1 = 0.1739 \rightarrow \mathrm{rms}\theta = 107°, f_\theta = 0.500\ \mathrm{cpy}, a_{IT} = 2.00\ \mathrm{cm}$$

and

$$\nu_2 = 0.3100 \rightarrow \mathrm{rms}\theta = 87.7°, f_\theta = 0.696\ \mathrm{cpy}, a_{IT} = 2.07\ \mathrm{cm}.$$

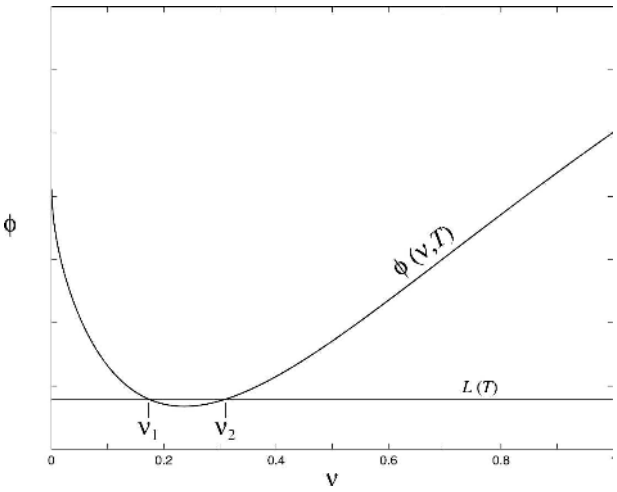

FIG. 8. Toy model plot of $\phi(\nu, T)$ for $T = 1240$ days. The intersection with $L(T)$ gives two roots; ν_2 depends on the record length and is unphysical.

The first root yields the assumed model values. The second has smaller rms θ at larger f_θ (but similar $\dot{\theta}$); the two models have indistinguishable $S_h(f)$ spectra but wildly different $S_\theta(f)$ spectra. Taking $T = 620$ days (one-half of the previous length) gives $\nu_1 = 0.1739$ and $\nu_2 = 0.340$; thus, the second root is eliminated by noting that it (improperly) varies with record length.

c. N_2 to the rescue?

An independent determination (the sixth equation for the six unknowns) can be made on the assumption that the (complex) admittance of the surface tide relative to the equilibrium tide should be nearly the same for constituents at neighboring frequencies, as indeed indicated in the bottom panel of Fig. 2.

Here difficulties are encountered because of the overlap of bands from neighboring constituents. Such problems had previously been encountered for the left skirt of the M_2 band, being partly hidden beneath the center of the N_2 band, making it difficult to estimate the total energy $E_{M_2}^{\mathrm{BAND}}$; this overlap is a source of error in the analysis so far. A much greater difficulty is encountered in trying to extract the relatively weak N_2 band in the presence of its powerful M_2 neighbor.

This heroic effort to close the gap of five equations in six unknowns was abandoned in favor of the limited goal for only three parameters, a_{IT}, rms(θ), and f_θ. The remaining three parameters can be estimated from a Cartesian analysis. The subject of tides is most simply formulated in the frequency domain, however, and there is a price to pay for abandoning the explicit relations with identified constituents. Here the interpretation of the Hawaiian records depends on a parallel

analysis in the frequency domain and the forthcoming Cartesian time domain analysis.

4. Cartesian domain

Dropping the restriction of a Lorentzian phase spectrum and eliminating f_θ as an explicit unknown leaves five unknowns to be evaluated using five observables.[6] The Cartesian analysis examines the statistical properties of the amplitudes of the real and imaginary components of Eq. (31):

$$X(t) = a_{\rm ST}\cos\theta_{\rm ST} + a_{\rm IT}\cos[\theta_{\rm IT} + \theta(t)] \quad \text{and}$$
$$Y(t) = -a_{\rm ST}\sin\theta_{\rm ST} - a_{\rm IT}\sin[\theta_{\rm IT} + \theta(t)]. \tag{47}$$

a. Demodulate statistics

The standard proceedure is to perform a complex demodulation of $h(t)$ at the carrier frequency f_c:

$$h(t;f_c) = \frac{1}{T}\int_{-T/2}^{T/2} dt' h(t' - t)e^{-i2\pi f_c(t'-t)} \tag{48}$$

$$= a_{\rm ST}e^{-i\theta_{\rm ST}} + \frac{a_{\rm IT}e^{-i\theta_{\rm IT}}}{T}\int_{-T/2}^{T/2} dt'\, e^{-i\theta(t'-t)} \tag{49}$$

$$\simeq X(t) + iY(t), \tag{50}$$

as defined in Eq. (47), provided T is small relative to the characteristic time scale of $\theta(t)$. In the application to the toy model where the carrier is a pure tone at f_c, the aforementioned demodulation scheme is entirely appropriate. However, for real ocean tides the M_2 "carrier" is itself modulated by additional celestial factors, thus necessitating the requirement for a new demodulation approach. This is discussed in section 5b.

The smallest record length that will separate tidal constituents is the lunar month, or $T = 27.321\,582$ days. For improved discrimination, a Hanning window with T of roughly two lunar months was used; that is, $T \equiv 106$ M_2 cycles and $T \simeq 104$ N_2 cycles. An estimate of $h(t;f_c)$ for every $\Delta t = T/2$ yields a nearly monthly time series of demodulates.

The polar angle ψ and total amplitude $a_{\rm TT}$ are given by

$$\psi(t) = \tan^{-1}Y(t)/X(t) = -\tan^{-1}\left\{\frac{a_{\rm ST}\sin\theta_{\rm ST} + a_{\rm IT}\sin[\theta_{\rm IT} + \theta(t)]}{a_{\rm ST}\cos\theta_{\rm ST} + a_{\rm IT}\cos[\theta_{\rm IT} + \theta(t)]}\right\} \tag{51}$$

and

$$a_{\rm TT}(t) = (X^2 + Y^2)^{1/2} = \{a_{\rm ST}^2 + a_{\rm IT}^2 + 2a_{\rm ST}a_{\rm IT}\cos[\theta_{\rm ST} - \theta_{\rm IT} - \theta(t)]\}^{1/2}. \tag{52}$$

The model has a constant $a_{\rm IT}$, yet the total amplitude $a_{\rm TT}$ is modulated in time by the variable phase. Expectation values for the Cartesian components under the Gaussian phase assumption are

$$\langle X\rangle = a_{\rm ST}\cos\theta_{\rm ST} + a_{\rm IT}\nu\cos\theta_{\rm IT} \quad \text{and}$$
$$\langle Y\rangle = -a_{\rm ST}\sin\theta_{\rm ST} - a_{\rm IT}\nu\sin\theta_{\rm IT}, \tag{53}$$

where $\nu^2 = \exp(-\overline{\theta^2})$ as before. In accord with Eq. (33) the mean polar angle is $\langle\psi\rangle = \tan^{-1}\langle Y\rangle/\langle X\rangle$.

The three second-order Cartesian statistics are crucial to this analysis:

$$\langle X^2\rangle = a_{\rm ST}^2\cos^2\theta_{\rm ST} + 2a_{\rm ST}a_{\rm IT}\nu\cos\theta_{\rm ST}\cos\theta_{\rm IT} + \frac{a_{\rm IT}^2}{2}(1 + \nu^4\cos2\theta_{\rm IT}), \tag{54}$$

$$\langle Y^2\rangle = a_{\rm ST}^2\sin^2\theta_{\rm ST} + 2a_{\rm ST}a_{\rm IT}\nu\sin\theta_{\rm ST}\sin\theta_{\rm IT} + \frac{a_{\rm IT}^2}{2}(1 - \nu^4\cos2\theta_{\rm IT}), \quad \text{and} \tag{55}$$

$$\langle XY\rangle = -\frac{1}{2}[a_{\rm ST}^2\sin2\theta_{\rm ST} + 2a_{\rm ST}a_{\rm IT}\nu\sin(\theta_{\rm ST} + \theta_{\rm IT}) + a_{\rm IT}^2\nu^4\sin2\theta_{\rm IT}]. \tag{56}$$

The total energy [consistent with Eqs. (35) and (41)] is

$$E = E^{\rm LINE} + E^{\rm BAND} = \frac{1}{2}(\langle X^2\rangle + \langle Y^2\rangle) = \frac{1}{2}[a_{\rm ST}^2 + a_{\rm IT}^2 + 2a_{\rm ST}a_{\rm IT}\nu\cos(\theta_{\rm ST} - \theta_{\rm IT})]. \tag{57}$$

The band energy is given by

$$E^{\rm BAND} = \frac{1}{2}(\sigma_X^2 + \sigma_Y^2) = \frac{1}{2}a_{\rm IT}^2(1 - \nu^2), \tag{58}$$

where

$$\sigma_X^2 = \langle X^2\rangle - \langle X^2\rangle \quad \text{and} \quad \sigma_Y^2 = \langle Y^2\rangle - \langle Y\rangle^2. \tag{59}$$

b. Parameter estimates for a toy model

The five Cartesian moments $\langle X\rangle$, $\langle Y\rangle$, $\langle X^2\rangle$, $\langle Y^2\rangle$, and $\langle XY\rangle$ are used to derive the five parameters $a_{\rm ST}$, $\theta_{\rm ST}$, $a_{\rm IT}$, $\theta_{\rm IT}$, and ν. Two auxiliary observables,

[6] The frequency scale of the modulation can subsequently be inferred from an inspection of the demodulated internal tide record by noting that the Lorentzian spectrum has one-half of the total variance between $f = 0$ and $f = f_\theta$.

$$A = \frac{1}{2}(\sigma_X^2 + \sigma_Y^2) = \frac{1}{2}(1 - \nu^2)a_{\rm IT}^2 \quad \text{and}$$
$$B = \langle XY\rangle - \langle X\rangle\langle Y\rangle = \frac{1}{2}a_{\rm IT}^2\nu^2(1 - \nu^2)\sin(2\theta_{\rm IT}), \tag{60}$$

and Eqs. (53)–(56) yield $a_{\rm IT}(\nu)$ and $\theta_{\rm IT}(\nu)$. Note that the quantities A and B impose a minimum value of $\nu_{\rm min} = (|B/A|)^{1/2}$. Because of the ambiguity associated with the $\sin(2\theta_{\rm IT})$ there are four more possible values of $\theta_{\rm IT}(\nu)$, given by

$$\theta'_{\rm IT} = (\pm\pi/2 - \theta_{\rm IT}) \quad \text{and} \quad (\pm\pi + \theta_{\rm IT}). \tag{61}$$

For each $\theta_{\rm IT}(\nu)$ value, two new functions,

$$C(\nu) = \langle X\rangle - \nu a_{\rm IT}(\nu)\cos\theta_{\rm IT}(\nu) = a_{\rm ST}\cos\theta_{\rm ST} \quad \text{and}$$
$$D(\nu) = \langle Y\rangle - \nu a_{\rm IT}(\nu)\sin\theta_{\rm IT}(\nu) = a_{\rm ST}\sin\theta_{\rm ST}, \tag{62}$$

are formed, thereby yielding equations for $a_{\rm ST}(\nu)$ and $\theta_{\rm ST}(\nu)$. Equations (60) and (62) conveniently express the four parameters $a_{\rm ST}$, $\theta_{\rm ST}$, $a_{\rm IT}$, and $\theta_{\rm IT}$ solely as a function of the fifth parameter, ν. The best solution is determined by least squares analysis. A trial demodulate time series is constructed by estimating the internal tide phase time series using

$$\theta(t;\nu) = -{\rm Im}(\ln\{[h(t;f_c) - a_{\rm ST}(\nu)e^{-i\theta_{\rm ST}(\nu)}]e^{i\theta_{\rm IT}(\nu)}/a_{\rm IT}(\nu)\}) \tag{63}$$

so that

$$h_{\rm trial}(t;\nu) = X_{\rm trial}(t;\nu) + iY_{\rm trial}(t;\nu)$$
$$= a_{\rm ST}(\nu)e^{-i\theta_{\rm ST}(\nu)} + a_{\rm IT}(\nu)e^{-i[\theta_{\rm IT}(\nu)+\theta(t;\nu)]}. \tag{64}$$

The best solution yields a minimum for the objective function

$$J^2(\nu) = \langle(X - X_{\rm trial})^2\rangle/\sigma_X^2 + \langle(Y - Y_{\rm trial})^2\rangle/\sigma_Y^2,$$
$$\nu_{\rm min} < \nu < 1, \tag{65}$$

where the ensemble averages are defined as a mean over time (see appendix D for details).

The resulting parameter estimates for the toy model (Table 1, row b) fall significantly short of the assumed values; the time series is restricted to the M_2 band, thus neglecting the considerable energy that spills beyond the neighboring constituents. This is an inevitable complexity arising from the fact that the frequency splitting associated with celestial orbits (cpm, cpy) is not well separated from the frequency scale of the ocean-induced phase modulation. In developing a procedure to correct for this shortfall, the toy model serves as guidance to the subsequent Honolulu and Hilo analyses.

In the frequency domain the procedure is relatively straightforward (and has been incorporated in Table 1, row a); it consists of fitting the inner uncontaminated frequency bins by Eq. (27) (assuming a Lorentzian phase spectrum) and then using the fitted curve to extrapolate into and beyond the neighboring constituents. In the time domain the procedure is more complex (appendix D). The corrected values (Table 1, row c) are now reasonably close to the assumed parameters.

5. Honolulu and Hilo

Hourly Honolulu (1905–2000) and Hilo (1927–2000) tide records were obtained from the University of Hawaii Sea Level Center (courtesy of M. Merrifield). Record gaps and obvious tsunami events were replaced by response-method predictions (Munk and Cartwright 1966; gravitational potential only).[7] The hourly data were then low-pass filtered to remove energy with periods less than 6 h, and as a last step the data were interpolated and decimated to give exactly four samples per M_2 period.

Table 1 summarizes the derived parameters for the Honolulu and Hilo records. The procedure follows closely the methods developed and tested with the toy model, but there is an important difference. Whereas in the toy model the carrier was a "pure" tone at f_c = 1.932 274 6 cpd frequency, the M_2 "carrier" is itself modulated by the orbital perturbations of monthly, yearly, and nodal frequencies. Modification of the procedure followed for the toy model follows along two lines. In the frequency domain the band energy is taken as that fraction of the measured energy that is incoherent with the gravitational potential $h_g(t)$. In the Cartesian time domain the complex demodulation is performed with this gravitational potential carrier, which has all the orbital "impurities" built in. The function $h_g(t)$ can be generated hour by hour from the ephemerides of the earth–moon–sun system. This is the essence of the "response method" of tide prediction (Munk and Cartwright 1966).

a. Frequency domain

Figure 9 shows the high-resolution frequency spectra of the measured (solid circles) and incoherent fractions

[7] The response method predictions were estimated using the longest gap-free sections of the records, which for Honolulu was 1 January 1954–1 January 1962 and for Hilo was 1 January 1982–1 October 1999. The first 10 years of the Honolulu record show some unusual M_2 modulation (Fig. 2), so only data between 1915 and 2000 were used in the analysis. The Hilo record, although starting in 1927, had a large gap between 1935 and 1947, so we only used data between 1947 and 2000.

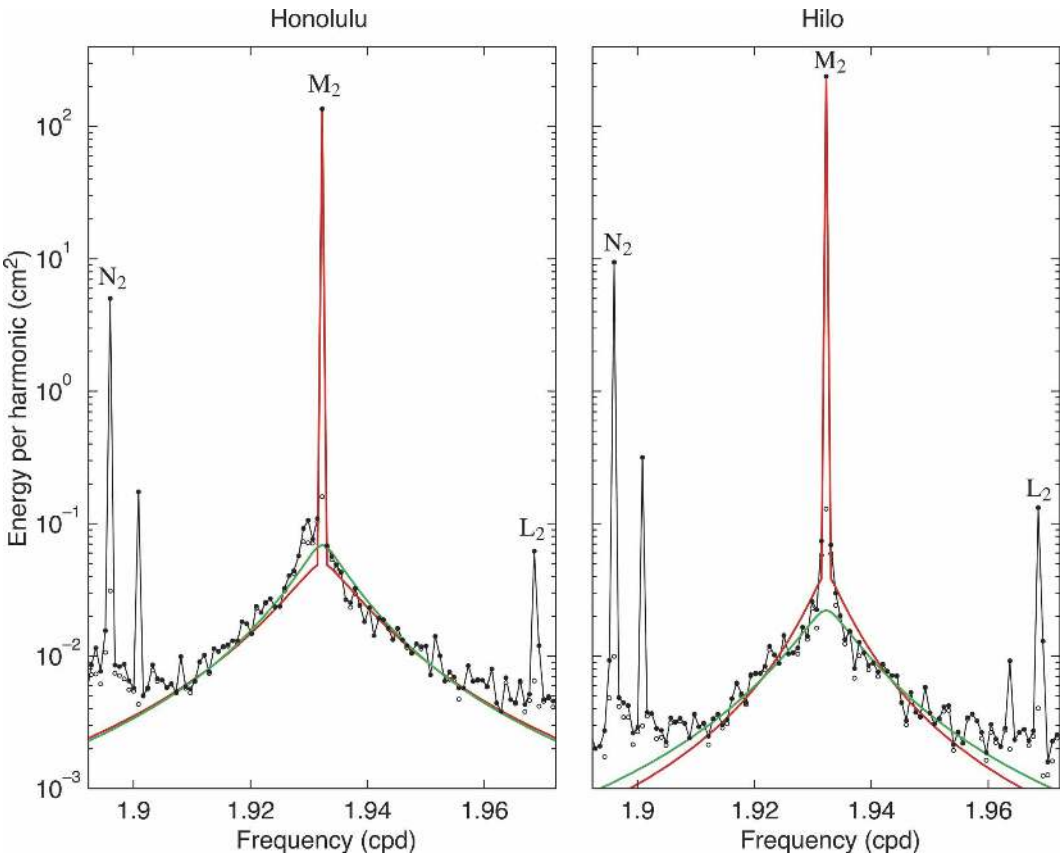

FIG. 9. High-resolution frequency spectra ($T = 1240$ days). The black dots and connecting lines are the measured E_j energies at M_2 frequency and adjoining harmonics; open circles (which mostly overlap) give the incoherent fraction. Neighboring constituents N_2 and L_2 (at cpm splitting) limit the M_2 analysis to harmonics between $j = -34$ to $j = +34$. Harmonics $j = 0$ and $j = \pm 1$ (for Hilo) require special consideration (see text). Green and red curves represent fits in the frequency domain and Cartesian time domain, respectively (Table 1, rows a and c).

(open circles) of tidal energy. The incoherent faction equals $(1 - \gamma^2)$ of the recorded energy $\langle H_{\rm rec}(j)H^*_{\rm rec}(j)\rangle$, where

$$\gamma^2(j) = \frac{|\langle H_{\rm rec}H^*_g\rangle|^2}{\langle H_{\rm rec}H^*_{\rm rec}(j)\rangle\langle H_gH^*_g(j)\rangle} \tag{66}$$

is the coherence, with $H_{\rm rec}$ and H_g designating the complex Fourier components of the tide record and the gravitational potential, respectively. The Fourier components were computed by dividing the records into as many 1/2-overlapping sections as possible for the assumed T. Each section was detrended (but not windowed) before being Fourier transformed. The ensemble angle brackets signify averaging the overlapping sections.

The spectra (Fig. 9) clearly show interference from neighboring constituents N_2 and L_2 (at cpm splitting) contaminating the M^2 band outside the harmonics $j = \pm 34$. Within the uncontaminated band nearly all of the measured E_j energy is incoherent except at $j = 0$ where the incoherent fraction is minute and poorly measured. The model fits over the uncontaminated bins allow extrapolation into and beyond the neigboring constituents.

For Hilo the bands, $j = \pm 1$, are abnormally energetic. The existence of an inner band of high energy is confirmed by higher-resolution analysis. The bandwidth is roughly 1/1240 day and the energy is 0.08 cm^2, small relative to the outer band energy of 0.65 cm^2. The subsequent Cartesian analysis can accommodate this small inner band since there is no assumption of a single (Lorentzian) band structure.

Traditional tidal analysis is in the frequency domain, with $E^{\rm LINE}$ entirely ascribed to the surface tide amplitude and the phase given by the record phase at the appropriate frequency. Equations (33) and (35) allow the estimate of error bars associated with the internal tide fluctuations (Table 1).

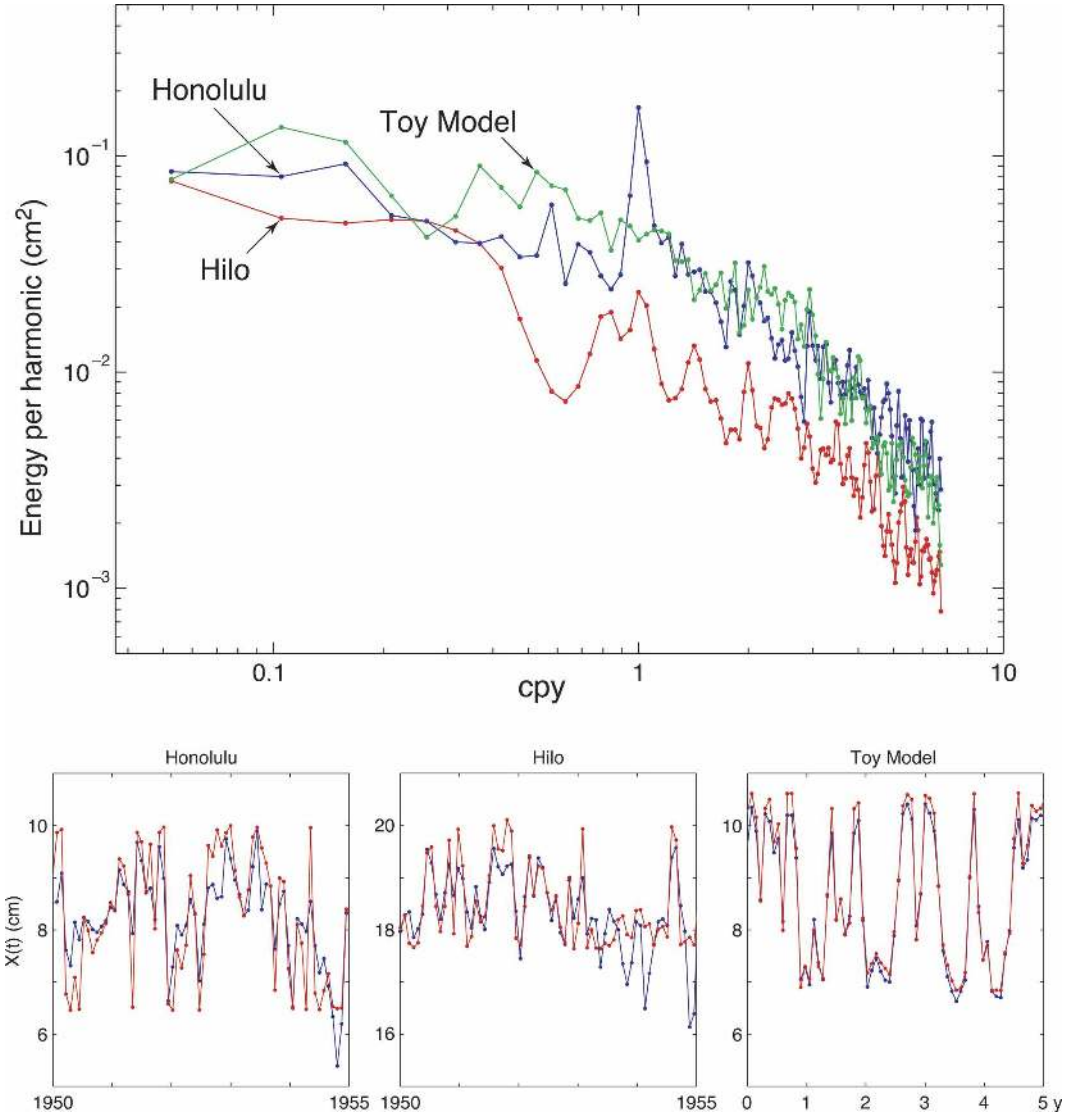

FIG. 10. (top) Cartesian frequency spectra. The plotted spectra are the sum of the X and Y spectra. (bottom) Blue dots and connecting lines are the demodulated time series; red dots and connecting lines are model fits.

b. Cartesian domain

The procedure is to demodulate the tide record and gravitational potential separately at the carrier f_c [Eq. (48)] giving $h_{\rm rec}(t;f_c)$ and $h_g(t;f_c)$. The demodulate value, accounting for all astronomical perpurbations to the M_2 group phase, is

$$h(t;f_c) = h_{\rm rec}(t;f_c)h_g^*(t;f_c)/|h_g(t;f_c)| \equiv X(t) + iY(t). \tag{67}$$

Perturbations to the demodulate amplitudes are treated separately by fitting (and removing) an 18.6-yr cycle.

Table 1 summarizes the results of the Honolulu and Hilo Cartesian analysis; the observed and modeled [Eq. (64)] time series of $X(t)$ are close (Fig. 10). For Honolulu and Hilo $J^2_{\rm min}$ has values of 0.43 and 0.44, respectively, accounting for roughly 80% of the $X(t)$ variance. On the other hand, the mean internal tide phase is very poorly determined because the phase variance is relatively high [resulting in a large uncertainty for a small value for B (Table 1)]. Interestingly, the Cartesian and frequency analyses yield very close values for the parameters $a_{\rm IT}$, rms θ, and f_θ, and Fig. 9 shows the close agreement of the frequency spectra. These results suggest that the Lorentzian assumption is not overly restrictive.

Figure 10 shows the frequency spectra of the Carte-

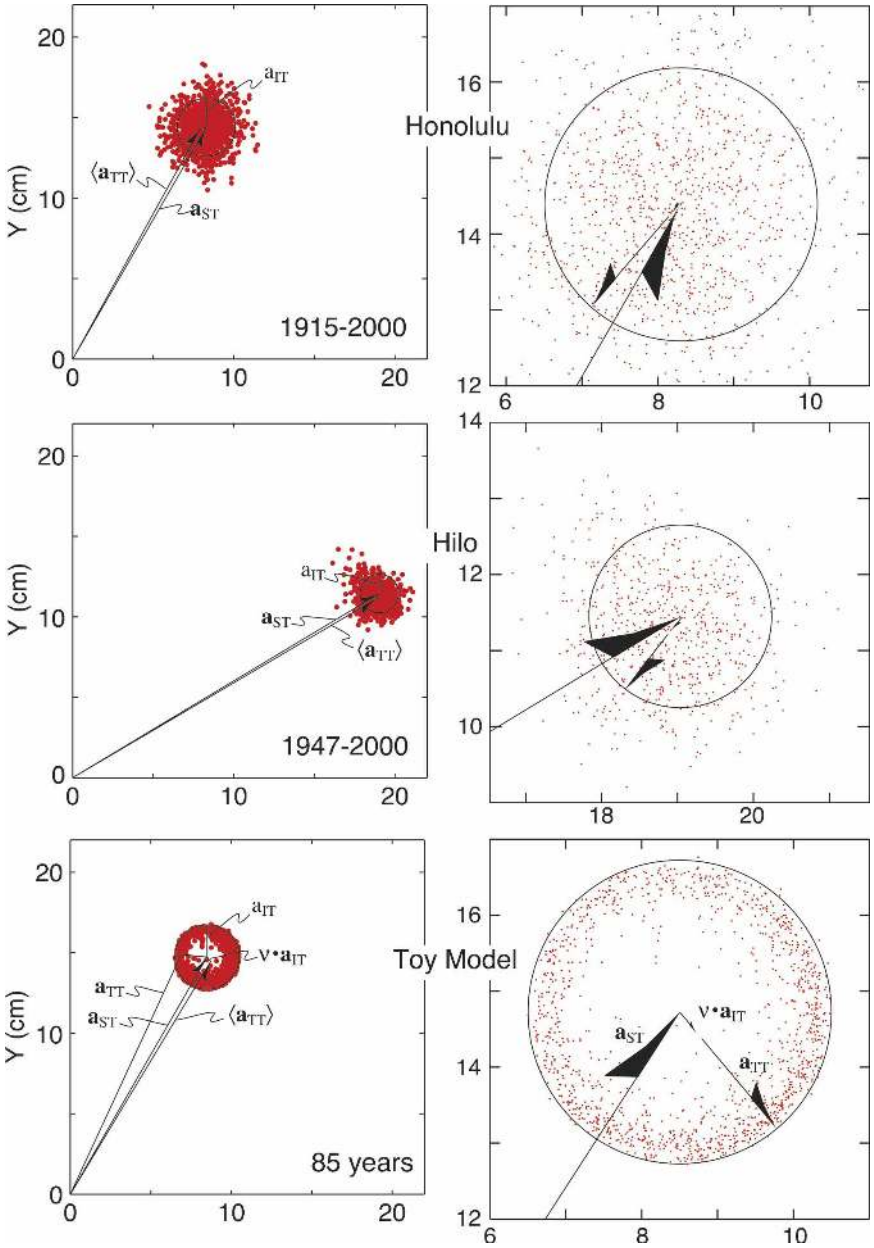

FIG. 11. Phasor diagram. The instantaneous total tide is the vector sum of the surface tide and the instantaneous internal tide: $\mathbf{a}_{TT} = \mathbf{a}_{ST} + \mathbf{a}_{IT}$. For phase modulation only, the $\mathbf{a}_{IT}$ vectors terminate along a circle of radius a_{IT}, as shown. Dots are monthly means. The weighted center defines the mean total tidal "constant" $\langle \mathbf{a}_{TT} \rangle = \mathbf{a}_{ST} + \langle \mathbf{a}_{IT} \rangle$.

sian time series. The Honolulu spectrum closely resembles the toy model spectrum except for the large annual peak. The Hilo spectrum does not show such a strong annual peak, and the overall energy is lower than Honolulu. The high-frequency ends of the spectra all look very similar with a roughly f^{-2} dependence, which gives confidence in our "Lorentzian" correction to the Cartesian parameters for the high-frequency variability (Table 1).

c. *Phasor diagrams*

The situation is neatly summarized in a phasor diagram (Fig. 11); dots refer to the phasor ($\mathbf{a}_{TT}$) averaged over one month. The *instantaneous* total tide is the sum of the instantaneous surface and internal tide vectors: $\mathbf{a}_{TT}(t) = \mathbf{a}_{ST} + \mathbf{a}_{IT}(t)$. Under the assumption of a pure phase modulation the phasor diagram is confined to a circular arc of radius a_{IT} centered on $\mathbf{a}_{ST}$. The mean of

all points is at $\langle \mathbf{a}_{TT} \rangle = (\langle X \rangle, \langle Y \rangle)$ [Eq. (53)]. Traditional tidal constants refer to the amplitude and phase angle of $\langle \mathbf{a}_{TT} \rangle$. In the limit $\nu \to 0$, demodulated points uniformly populate a complete circle centered on $\mathbf{a}_{ST}$, and in the limit $\nu \to 1$ demodulated points are closely clustered along a narrow arc in the direction of θ_{IT} (thus pulling $\langle \mathbf{a}_{TT} \rangle$ away from $\mathbf{a}_{ST}$). A dominant amplitude modulation has a very different phasor diagram; it is lined up along a narrow radial strip in the direction of the internal tide vector.

The demodulation is not instantaneous but occurs over some time interval T_d. If the internal tide phase is changing over the time T_d, then the points in the phasor display are no longer bound to the arc of radius $\mathbf{a}_{IT}$ but penetrate the interior (but may not escape to the arc exterior). Figure 11 shows this type of infilling for the pure phase modulation of the toy model.

The Hawaii phasor plots are not consistent with amplitude modulation, nor do they exhibit the circular crescent associated with an exclusive phase modulation. The mean internal phase θ_{IT} is very poorly determined. Despite these shortcomings the pure phase modulation model does account for nearly 80% of the Cartesian variance, but the lack of resemblance between the measured and toy phasors is disconcerting.

The residual 20% variation can be placed in two categories: one in which the center of the arc is infilled and one in which the points escape the arc exterior (outfilling). Phase modulation at time scales short relative to $T_d = 1$ month (such as the energetic fortnightly modulation) contribute to the infilling. Interference phenomena from multiple internal tide sources and/or modes can contribute to both infilling (destructive interference) and outfilling (constructive interference). Amplitude modulation may contribute to both infilling and outfilling. Last, there is the effect of an uncorrelated measurement noise, but the component time series (Fig. 10) does not resemble uncorrelated noise.

6. Discussion

The previous results are evidence for a significant internal M_2 tide component, roughly 10% in Honolulu and 6% in Hilo. The *internal* tide, particularly its phase, is strongly modulated by upper-ocean processes. The modulation of the *surface* tide is negligible. The recorded *total* tide, $\mathbf{a}_{TT}(t) = \mathbf{a}_{ST} + \mathbf{a}_{IT}(t)$, is a (vector) sum of the dominating nonmodulated surface tide and the small but strongly modulated internal tide. Accordingly, the total tide is weakly modulated, as indicated by small irregularities in the recorded tidal "constants" (Fig. 2), offering a welcome window into past ocean variability.

a. Baroclinic "corruption" of tide records

This effect should come as no surprise; it is an inevitable consequence of an environment of strong coupling between barotropic and baroclinic processes. It has long been known that efforts to measure barotropic tidal currents from a string of moored current meters are greatly hampered by the superposition of the baroclinic tidal currents of comparable magnitude; a major effort of vertical and horizontal averaging is required to extract accurate barotropic tidal current constants. Referring to previous measurements by Ekman and Helland-Hansen (1931) and Defant (1932), Sverdrup et al. (1942, p. 594) remark, "observations from different depths show that tidal periods dominate, but, instead of being uniform from surface to bottom as would be expected if the currents were ordinary tidal currents, the amplitude and time of maximum current (the phase) vary in a complicated manner."

This coincidence in the magnitude of the barotropic and baroclinic kinetic energies is associated with the strong scattering interaction and resulting partition of energy between modes. One-third of the global surface tide dissipation is associated with the scattering of surface tides into internal tides, 1 TW out of 3 TW. Global energy in the surface tides is about 4×10^5 TJ (roughly 10^5 J m^{-2}) and is comparable to the internal tidal energy now estimated at a few times 10^5 TJ (Munk and Wunsch 1998).

The partition of energy is all that is needed to estimate the relative surface amplitudes:

$$E_{IT} = cE_{ST}, \quad \text{where} \quad c = O(\text{unity}). \tag{68}$$

Let a_{ST} designate the amplitude of the surface tide and a_{IT} be the surface manifestation of an internal tide of internal amplitude A_{IT}. For a two-layer system with density contrast $\Delta\rho$,

$$E_{ST} = \frac{1}{2}\rho g\, a_{ST}^2 \quad \text{and} \quad E_{IT} = \frac{1}{2}\Delta\rho g\, A_{IT}^2. \tag{69}$$

For a thin upper layer relative to bottom depth ($H \ll D$) and weak density contrast ($\Delta\rho \ll \rho$), the ratio of surface to interior displacement is (Gill 1982, p. 122)

$$\frac{a_{IT}}{A_{IT}} = -\frac{\Delta\rho}{\rho}\left(1 - \frac{H}{D} + \cdots\right). \tag{70}$$

Combining Eq. (68) with Eq. (70) yields

$$|a_{IT}| \approx |a_{ST}|\sqrt{\frac{c\Delta\rho}{\rho}}. \tag{71}$$

For constant $N^2 = (g/\rho)d\rho/dz$ in water of depth D, the internal wave mode 1 at frequency $\omega \ll N$ has a relative surface displacement [Eq. (E7)]

$$\frac{a_{IT}}{A_{IT}} = -\pi^{-1}\Delta\rho/\rho \tag{72}$$

with $\Delta\rho = (d\rho/dz)D$ now designating bottom minus surface density; Eq. (72) is of similar form as the two-layer case Eq. (70), leading again to a relation of form Eq. (71).

Neither the two-layer nor the constant-N model can claim reality; the two models present opposite extremes of stratification, and we surmise that quite generally the expected surface amplitude of internal tides is of order $\sqrt{\Delta\rho/\rho}$ times the amplitude of surface tides. For orientation, setting $\Delta\rho/\rho = 10^{-3}$ and tidal energy densities $E_{ST} = E_{IT} = 10^3$ J m^{-2} yields $a_{ST} = 50$ cm, $A_{IT} = 15$m, and $a_{IT} = 1.5$ cm, consistent with Table 1.

Variability in the values of tidal "constants" should be the rule rather than the exception! Cartwright (1972) analyzed the tide record from 1711 to 1936 at Brest, France, and found a 1% (100 yr)$^{-1}$ decrease in the semidiurnal amplitude. He could not determine whether the changes were oceanic or local in origin, but he eliminated harbor development as a major factor. Flick et al. (2003) have compiled mean high water (MHW), mean low water (MLW), mean sea level (MSL), and other statistics for 87 U.S. stations of more than 20 years in duration. The M_2 amplitudes are inferred from ½(MHW–MLW). About one-half of the stations show significant (positive or negative) trends. Representative values are +4.7 cm (100 yr)$^{-1}$ for La Jolla, −1 cm (100 yr)$^{-1}$ for Woods Hole, +0.9 cm (100 yr)$^{-1}$ for Honolulu, and +1.5 cm (100 yr)$^{-1}$ for Hilo.

b. Removing the ground motion

The *residual* Honolulu and Hilo tide records, after subtraction of tidal effects, are dominated by a secular trend (Fig. 12). The mean trends have large contributions from ground motion associated with volcanic and tectonic activity. The removal of ground motion is a major consideration in the analysis of the tide records.

Many factors may contribute to land subsidence or uplift at coastal tide gauges, including large-scale lithospheric flexure (in Hawaii caused by buoyant mantle plumes) and local seismicity. GPS recorders collocated with the gauges offer the best hope to resolve these land motions, but the time series are noisy and are only a few years old (M. A. Merrifield 2002, personal communication). Estimates of vertical motion must therefore depend on more indirect methods. On the island of Hawaii radiometric dating of drowned coral reefs (Moore and Fornari 1984; Moore and Clague 1992) suggests a subsidence of about 26 cm (100 yr)$^{-1}$ over the last 500 000 years. A drill hole near Hilo (Moore et al. 1996) suggests a similar rate of about 22 cm (100 yr)$^{-1}$ over the last 40 000 years.

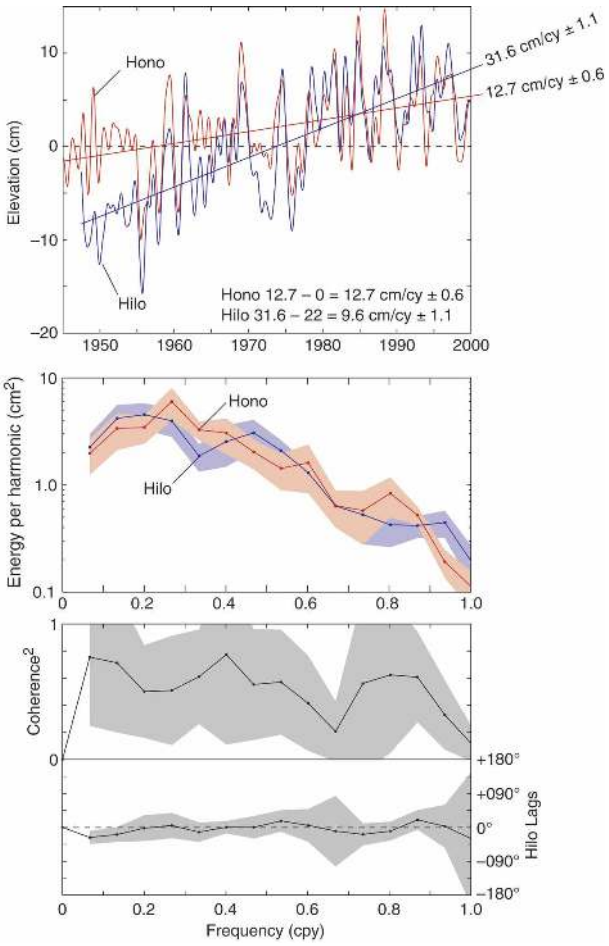

FIG. 12. (top) Honolulu and Hilo mean sea level without geodetic correction. Series have been low-pass filtered with a cutoff frequency 1 cpy, and the mean annual cycle has been removed. The corrected sea level rise is by 12.7 and 9.6 cm (100 yr)$^{-1}$, respectively. The correlation coefficient is 0.75 for the total records and 0.74 after removal of the trends (the expected value for truly uncorrelated data is 0.32). (middle) Spectra of the detrended sea level in centimeters squared per harmonic (resolution $\delta f = 0.067$ cpy), with 65% confidence limits. (bottom) Squared coherence and Hilo phase lag relative to Honolulu. The $T = 53$ yr joint record length provides seven degrees of freedom.

Subsidence rates to the west of the island of Hawaii are expected to be smaller as the lithospheric flexure decreases away from this strongly forced "hot spot" region (Moore 1970). In fact, analysis of coral deposits and stratigraphic evidence within these deposits suggest that Lanai (200 km northwest of Hawaii) has experienced a small *uplift* at a rate of about 2 cm (100 yr)$^{-1}$ (Grigg and Jones 1997; Rubin et al. 2000). Uplifts at Lanai and Maui are consistent with a model of the lithopheric distortions "downstream" of the mantle plume (Zhong and Watts 2002). The same model leads to a negligible Oahu uplift of about 0.04 mm yr^{-1}

(Grigg and Jones 1997; Watts and ten Brink 1989; Zhong and Watts 2002), consistent also with the low seismicity under the island. The Oahu ground motion is much more in doubt than that in Hilo, but the required correction appears to be small.

Using 0 and 22 cm (100 yr)$^{-1}$ for the subsidence of the Honolulu and Hilo gauge sites leaves a residual rise by 12.7 and 9.6 cm (100 yr)$^{-1}$, respectively (Caccamise et al. 2005). The difference is not significant on account of the large uncertainties in the geodetic "corrections"; yet there is every reason to expect differences of this order as related to the variable circulation in the subtropical and equatorial Pacific Ocean. Superimposed on the secular trend is a large and correlated variability apparently associated with the waxing and waning of the North Pacific high (M. A. Merrifield and E. Firing 2003, personal communication). Coherence at the subannual frequencies lends credence to both time series; the low phase difference suggests forcing on a scale large in comparison with the island separation.

c. The Mitchum and Chiswell correlation

The detided sea level $h_{\rm SL}(t)$ and the M_2 tidal constituent amplitude $a_{\rm TT}(t)$ can be considered as independent time series, though both are derived from the same tide record. A surprising result discovered by Mitchum and Chiswell (2000) is that the two time series are correlated. This correlation plays a major role in our attempt to disentangle the record.

Figure 13 shows the Honolulu sea level $h_{\rm SL}(t)$ (now corrected for ground motion), the M_2 total amplitude $a_{\rm TT}(t)$, and their cross-spectra. The $a_{\rm TT}$ spectra are lower than the $h_{\rm SL}$ spectra by two orders of magnitude (we have plotted 10 $a_{\rm TT}$). The spectra are coherent and in phase between 0.2 and 0.5 cpy: tidal amplitude is high when sea level is high. Further, and quite independently, there is a secular trend in the M_2 amplitude by 1.1 cm (100 yr)$^{-1}$. The situation is similar for Hilo (Fig. 14) with a secular trend of 1.5 cm (100 yr)$^{-1}$.

Table 2 shows a consistency between the two stations and (remarkably) a resemblance at each station between the century trend and the subannual variability. Tidal amplitudes increase by order of 1 cm for a 10-cm rise in sea level, regardless of whether the rise is on an interannual or century time scale (more later).

d. Fitting the correlation

Figure 15 shows the various types of modulation that could account for the observed increase in the recorded M_2 amplitude. The simplest cases are those of a change in the internal amplitude only and the internal phase only. The third case of interference between two larger internal (but still small relative to the surface) components of nearly opposite phase would account for occasional fade-outs with π phase jumps. We proceed under the assumption that the Mitchum–Chiswell correlation is a result of an internal phase modulation.

Figure 16 shows parametric plots of the amplitude of the total M_2 constituent $a_{\rm TT}(t)$ versus the mean sea level $h_{\rm SL}(t)$ for the entire set of monthly means. The data are presented in two frequency bands: the "secular" band (0–0.1 cpy) and the interannual band (0.2–0.5 cpy). The similarity of the two patterns suggests that they are governed by the same ocean processes.

The secular increase in M_2 amplitude is now ascribed to a rotation of the IT vector associated with the rising sea level. Sea level is regarded as a proxy for thermocline depth (more generally for the interior density distribution). In any baroclinic model a *higher* sea level is accompanied by a *deeper* thermocline, which in turn leads to an *increase* in the IT phase velocity (section 6e) and a *decrease* in the internal phase lag between source and tide gauge:

$$\lambda \equiv d\phi/dh_{\rm SL} \tag{73}$$

is negative. (A deeper thermocline also implies a movement of the scattering source, which can either increase or decrease the shelf-to-shore phase difference.)

For the instantaneous tide vector

$$\mathbf{a}_{\rm TT}(t) = \mathbf{a}_{\rm ST} + \mathbf{a}_{\rm IT}(t) \tag{74}$$

we have, to order $\epsilon = a_{\rm IT}/a_{\rm ST}$,

$$a_{\rm TT} = a_{\rm ST} + a_{\rm IT}\cos\phi, \tag{75}$$

where $\phi(t) = \theta(t) + \theta_{\rm IT} - \theta_{\rm ST}$ is the lag of the internal tide relative to the surface tide. Writing

$$\phi(h_{SL}) = \pm\frac{\pi}{2} + \lambda(h_{SL} - h^*_{SL})\begin{cases}(+) & \text{for} \quad 0 < \phi < \pi \\ (-) & \text{for} \quad 0 > \phi > -\pi\end{cases} \tag{76}$$

identifies $h^*_{\rm SL}$ with the sea level when (if ever) $\delta a_{\rm TT} = a_{\rm TT} - a_{\rm ST} = 0$. A least squares fit to

$$\delta a_{\rm TT}(h_{\rm SL}) = \mp a_{\rm IT}\sin\lambda(h_{\rm SL} - h^*_{\rm SL}) \tag{77}$$

determines the parameters λ and $h^*_{\rm SL}$ (Table 3). The assumed relation accounts for about one-half of the variance, consistent with the order (0.5) squared coherences in Figs. 13 and 14.

For both Honolulu and Hilo high amplitude correlates with high sea level, and the upper sign in Eq. (77)

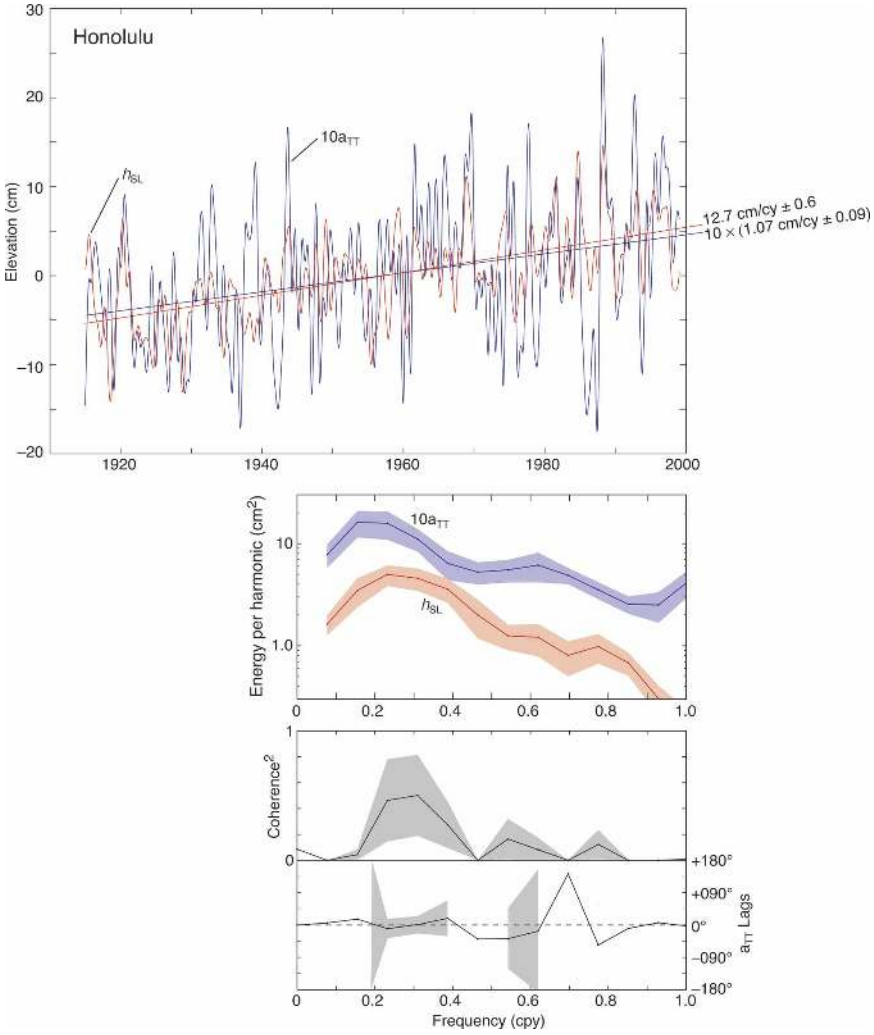

FIG. 13. Geodetically corrected Honolulu mean sea level vs 10 × amplitude of M_2 constituent, with $\delta f = 0.0774$ cpy, $T = 83$ yr, and degrees of freedom = 12 (see Fig. 15). Correlations are 0.52 and 0.42 before and after removal of trends, respectively, and the expected value for truly uncorrelated data is 0.24.

applies[8] (λ is negative); for Kahului, Maui, the correlation is negative (Table 1 of Mitchum and Chiswell 2000). Whatever the sign, unless ϕ is near 0 or π, any perturbation in sea level is accompanied by an instantaneous perturbation in amplitude, thus accounting for the near-zero phase difference in Figs. 13 and 14.

Table 4 gives the computed M_2 amplitudes and internal tide phases at the start and end of the tidal records, taking 12.7 and 9.6 cm (100 yr)$^{-1}$ for the sea level rise at Honolulu and Hilo, respectively. The increase in amplitude is by about 1 cm (100 yr)$^{-1}$ for both stations. The computed Greenwich epochs $\theta_{IT} = 141°$ and 117° for the year 2000 compare to 140° and 145° from a numerical simulation (M. A. Merrifield 2003, personal communication). Cartesian Honolulu and Hilo estimates (Table 1) of 229° ± 128° and 233° ± 108° are essentially useless because of the very large error bars.

Frequencies above 0.5 cpy (not included here) show no overall pattern. The lack of coherence is surprising. Measurement noise is not a significant consideration (Agnew 1986); even the weak sidebands (Fig. 9) are well above the neighboring noise level. Processes not yet identified must play a decisive role.

[8] There are some well-defined sequences in which a rising sea level over many months is accompanied by a *decrease* in the amplitude (and vice versa). Researchers M. A. Merrifield and M. Alford (2003, personal communication) suggest dual generation at each of the "channel entrances," Makapuu being more energetic. Negative da_{TT}/dh_{SL} could be from western sources.

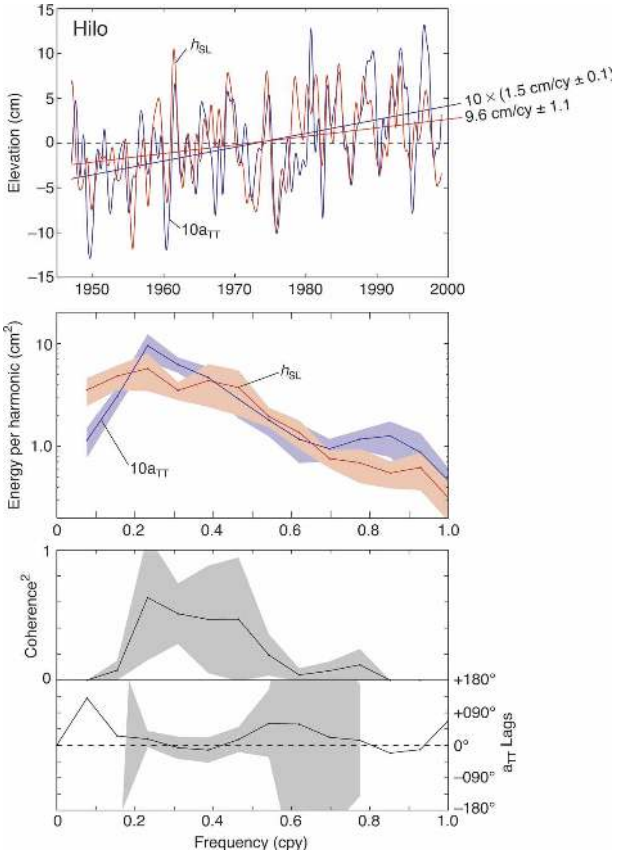

FIG. 14. Geodetically corrected Hilo mean sea level vs 10 × amplitude of M_2 constituent (see Fig. 15). Correlation is 0.62 and 0.56 before and after removal of trends, respectively, and the expected value for truly uncorrelated data is 0.32.

e. Internal tide modulation

Consider a long internal wave modulating an internal tide of much shorter wavelength (but still long relative to depth). Returning to the two-layer model, ζ_0 and ζ_{-H} are associated with the displacements in sea level h_{SL} and thermocline h_{TH} caused by the long modulating wave. The perturbed upper-layer thickness is [using Eq. (70)]

$$H(t) = H_0 + \delta H, \quad \text{where}$$
$$\delta H = h_{SL} - h_{TH} \approx -h_{TH} = +h_{SL}/(\Delta\rho/\rho).$$

For a thin layer H, the phase speed of the internal tide is simply

$$C_{IT}(t) = \sqrt{gH(t)\Delta\rho/\rho},$$

so

$$\frac{\delta C_{IT}}{C_{IT}} \simeq \frac{1}{2}\frac{\delta H}{H} = \frac{1}{2}\frac{h_{SL}/H}{\Delta\rho/\rho}. \tag{78}$$

Thus, to first order the fractional phase velocity perturbation scales as the vertical strain divided by the fractional density change.

Next, consider the perturbation from a vertical displacement $\zeta(z)$ in an $N(z)$ stratification. The resulting density perturbation follows from $\delta\rho = \zeta\, d\rho/dz$; quite generally,

$$\delta N^2 = N^2 d\zeta/dz + \zeta dN^2/dz \tag{79}$$

depends on the details of the stratification. The two terms are comparable and may be of opposite sign.

Next, consider subannual variability caused by low-frequency baroclinic Rossby waves. The vertical displacement of the Rossby waves $\zeta(z, t)$ modifies the interior density structure, which in turn modulates the phase speed $C_{IT}(t)$ of the internal tides. The slight surface displacement $\zeta(0, t)$ is associated with the recorded monthly mean sea level $h_{SL}(t)$. The two are related according to Eq. (E13):

$$\frac{\delta C_{IT}(t)}{C_{IT}} = \frac{1}{2}\pi^2 \frac{\mathrm{sinc}n}{1 - n^2/4}\frac{h_{SL}(t)/D}{\Delta\rho/\rho}, \tag{80}$$

where $\Delta\rho$ is the density change from bottom ($z = -D_{RO}$) to top ($z = 0$), and $n = D_{IT}/D_{RO}$, with $\mathrm{sinc}n = \sin\pi n/\pi n$. Rossby waves are long relative to the island dimensions, so D_{RO} is taken as 4.5 km, assuming that the resulting density perturbation reaches all the way to the coast into waters of depth $D < D_{RO}$. The internal tides are taken to travel within the coastal ocean along $D_{IT}(x) < D_{RO}$ and are subject to the Rossby perturbations.

The Rossby perturbation is a useful guide for mesoscale perturbation and possibly for the interannual variability; for the secular variation we consider the expected role of ocean warming. The *World Ocean Database* of five million temperature profiles (Levitus et al. 2000, 2001) has documented ocean warming since the mid-1950s, diminishing globally from about 0.15°C at 500 m to 0.03°C at 1000 m. There is no measurable change beneath 2000 m. For a density perturbation de-

TABLE 2. The M_2 amplitudes and sea level. Values in parentheses are from Flick et al. (2003).

	Secular trend		Energy/harmonic at 0.4 cpy		
	Honolulu	Hilo		Honolulu	Hilo
da_{TT}/dt [cm (100 yr)$^{-1}$]	1.1 (0.9)	1.5 (1.5)	E_{TT} (cm^2)	0.06	0.04
dh_{SL}/dt [cm (100 yr)$^{-1}$]	12.7 (12.9)	9.6 (12.0*)	E_{SL} (cm^2)	4	4
da_{TT}/dh_{SL}	0.09	0.16	$\sqrt{E_{TT}/E_{SL}}$	0.12	0.10

* After subtraction of 22 cm (100 yr)$^{-1}$.

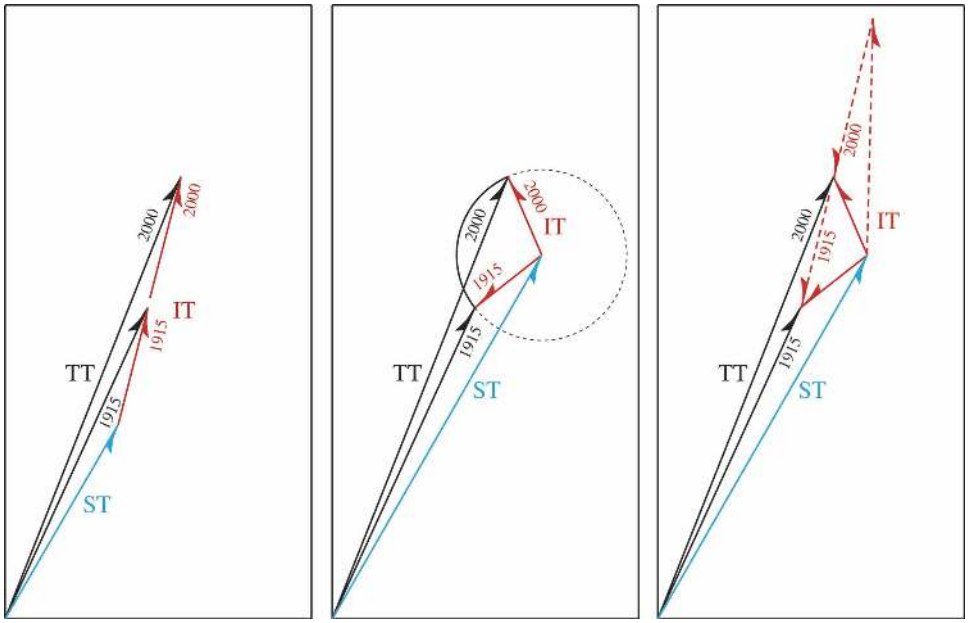

FIG. 15. Cartoons for the secular modification 1915–2000 of the recorded Honolulu M_2 tide vector. The total tide (black) is the sum of an invariable surface (blue) and variable internal (red) components, $\mathbf{a}_{TT} = \mathbf{a}_{ST} + \mathbf{a}_{IT}$. The simplest cases are those of a secular change in (left) amplitude only or (middle) phase only of the internal tide. (right) The interaction of two internal tide components (dashed) of nearly equal amplitude and nearly opposite phase, yielding a difference vector subject to fade-outs accompanied by π phase jumps.

creasing exponentially with depth z according to $\delta\rho/\rho = B \exp(-z/D_{TH})$, we have

$$h_{STERIC} = -\int_0^\infty dz\, \delta\rho/\rho = +D_{TH}B \quad \text{and}$$

$$\delta N^2 = -g\frac{d(\delta\rho/\rho)}{dz} = +\frac{gh_{STERIC}}{D_{TH}^2}e^{-z/D_{TH}},$$

so [using Eq. (E11)] for $\omega \ll N$,

$$\frac{\delta C_{IT}}{C_{IT}} = +\frac{1}{2}\frac{1-e^{-n}}{n(1+n^2/4\pi^2)}\frac{h_{STERIC}/D_{TH}}{\Delta\rho/\rho} \tag{81}$$

with $n = D_{IT}/D_{TH}$ and $\Delta\rho$ interpreted as the density difference between surface and the heat penetration depth. We associate the measured sea level rise with the "thermosteric" rise, $h_{SL} = h_{STERIC}$.

Accordingly, the relative phase change is

$$\frac{\delta\phi}{\phi} = -\frac{\delta C}{C} = -G\frac{h_{SL}/D}{\mathcal{D}\rho/\rho}, \quad \text{with} \tag{82}$$

$G = \frac{1}{2}, \frac{1}{2}\pi^2(1 + \text{order } n^2)$, and $\frac{1}{2}(1 - \frac{1}{2}n + \text{order } n^2)$ for the two-layer, Rossby, and global warming models. Here $n = D_{IT}/D$, where D_{IT} is the effective ocean depth for the internal tide propagation and D is the scale depth of Rossby wave propagation or buoyancy penetration; $\mathcal{D}\rho/\rho$ is the fractional density contrast between D and the surface. Equation (82) gives the rotation parameter $\lambda = \delta\phi/h_{SL}$ of the internal tide vector. Taking $D = 1$ km, $h_{SL} = 1$ cm, $\mathcal{D}\rho/\rho = 10^{-3}$, and $\phi = 360°$ (a distance of one wavelength between source and tide gauge[9]) gives $\lambda = -3.6°G\ \text{cm}^{-1}$ as compared with $-4°\ \text{cm}^{-1}$ in Table 3. It may come as a surprise that thermal expansion by a tiny δh_{SL} can play a comparable role to the much larger layer thickening in a Rossby wave perturbation [from a downward displacement of the lower boundary by $\delta h_{SL}/(\mathcal{D}\rho/\rho)$]. However, for a constant-N model with $C = HN/\pi$ and $\delta C/C = \delta H/H + (1/2)\delta N^2/N^2$, the second term dominates by a factor of $1/(\mathcal{D}\rho/\rho)$. The role of a weak buoyancy perturbation is amplified in a weakly stratified ocean!

Figure 17 shows the perturbations in stratification (δN^2) and internal tide phase speed ($\delta C/C$) as a function of water depth (D_{IT}) for the exponential warming and Rossby models; in both cases the surface displacement h_{SL} is taken at 10 cm. Here the phase speed perturbation is computed directly from the linear internal

[9] Simulations by P. Holloway and M. A. Merrifield (2003, personal communication) suggest an internal tide source region near Makapuu point, roughly 40 km east of Honolulu.

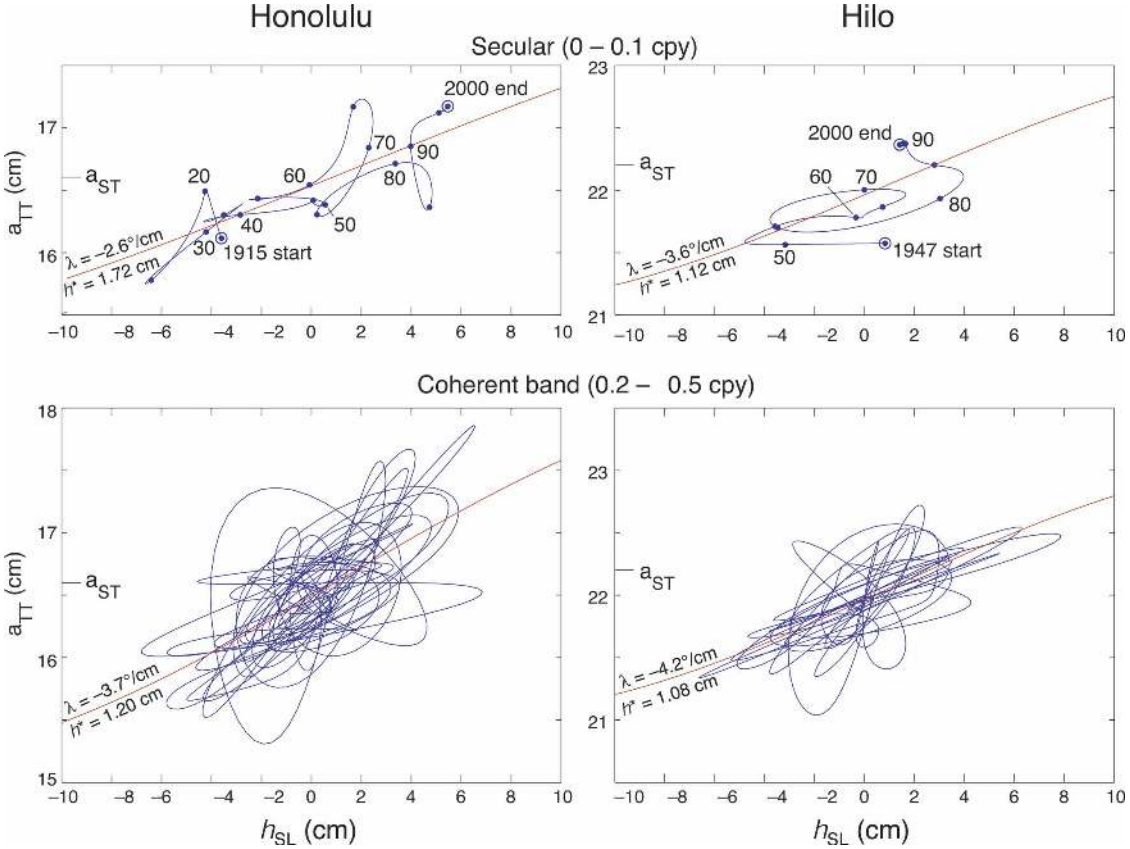

FIG. 16. Parametric plot (with 5-yr intervals indicated) of M_2 amplitude $a_{TT}(t)$ as function of the mean sea level $h_{SL}(t)$ (relative to midrecord and corrected for ground motion). Red curves are least squares fits to $a_{TT} = a_{ST} + a_{IT} \sin[\lambda(h_{SL} - h^*_{SL})]$, with surface and internal tide amplitudes taken from Table 1.

wave dynamics. The warming perturbation of C_{IT} exceeds the Rossby wave perturbation in deep water, whereas in very shallow water, of order several hundred meters, the perturbations are comparable. This result can account for the comparable magnitudes of the interannual and secular bands (Tables 2 and 3), a surprising result given the different physics of the Rossby and warming models. The conclusion is that the measured changes in sea level and in M_2 amplitude are consistent with the modulation of the internal tide by long Rossby waves and by a general warming of the water column.

TABLE 3. Least squares parameters predict about one-half of the variance.

	Secular (0–0.1 cpy)		0.2–0.5 cpy	
	Honolulu	Hilo	Honolulu	Hilo
λ(° cm^{-1})	−2.62 ± 0.11	−3.61 ± 0.20	−3.74 ± 0.17	−4.18 ± 0.23
h^*_{SL} (cm)	1.72 ± 0.14	1.12 ± 0.13	1.20 ± 0.11	1.08 ± 0.14
Variance (%)	58	54	49	50

f. Global sea level

In the previous section we have relied heavily on the changing sea level $h_{SL}(t)$ as a proxy for a changing density profile [which in turn affects the phase speed $C_{IT}(t)$ and thus the phase angle of the recorded internal tide]. *Measured* density profiles, 1950–2000, show significant warming in the waters surrounding the eastern Hawaiian Island chain (not shown), consistent with the estimates as inferred from $h_{SL}(t)$. This paper (for brevity) is restricted to the data provided by tide gauge records.

TABLE 4. Secular band (0–0.1 cpy) mean sea level and M_2 amplitude at the start and end of the Honolulu and Hilo tide records; ϕ is the phase of the internal tide relative to the surface tide, and θ_{IT} is the Greenwich phase.

	Honolulu		Hilo	
	1915	2000	1947	2000
h_{SL} (cm)	−5.4 ± 0.3	+5.4 ± 0.3	−2.5 ± 0.3	+2.5 ± 0.3
a_{TT} (cm)	16.05 ± 0.4	16.93 ± 0.4	21.78 ± 0.3	22.16 ± 0.3
ϕ	108.7 ± 1.0	80.4 ± 1.0	103.2 ± 1.2	85.2 ± 1.2
θ_{IT}	168.9 ± 1.0	140.6 ± 1.0	134.5 ± 1.2	116.5 ± 1.2

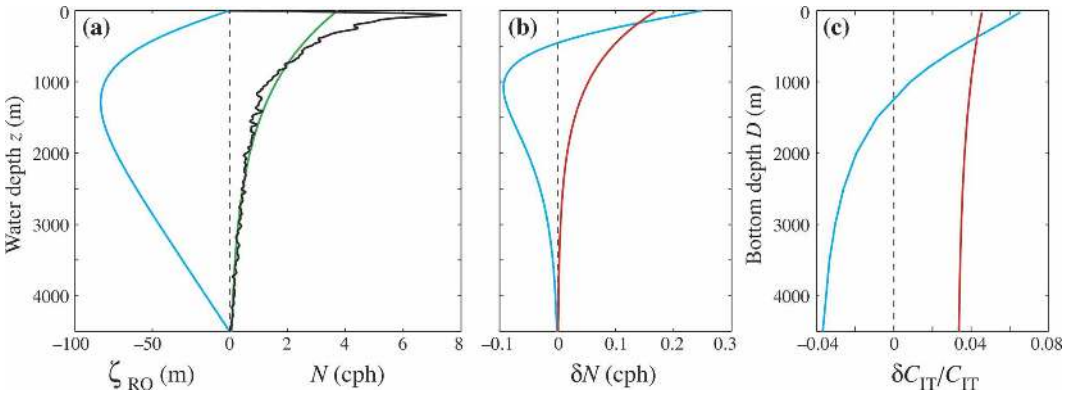

FIG. 17. (a) Exponential fit (green) to measured $N(z)$ profile (black) is associated with vertical displacement by $\zeta(z)$ of an internal Rossby wave (blue). (b) The resulting perturbation $\delta N(z)$ from the Rossby displacement (blue) and from a model of thermal expansion (red) are both consistent with a surface rise of 10 cm. (c) Resulting modulations of the phase speed of an internal tide for various depths D.

We could not resist a final implication of the Honolulu tide record. The availability of two time series, $h_{SL}(t)$ and $a_{TT}(t)$, permits us to place some restrictions on the various contributions to sea level rise, assuming that the recorded secular trend is representative of a global trend. Clearly, an imaginary 10 000-yr-old tide record showing a 20-m rise would be representative of global climate change, no matter where the tide gauge is located; a 10-yr record of a 0.1-m rise is not representative. What is the required record length to yield a sensible estimate of global change? Differences in elevation of order 1 m across major current systems are maintained geostrophically by the integrated wind stress on ocean basins. Variable differences of order ±10 cm can be expected because of the variable flux of momentum and buoyancy. To detect a sea level rise of 10 cm (100 yr)$^{-1}$ in the presence of 10-cm variable geostrophic topography requires a record length of order one century. A few venerable tide records might yield more information on global sea level than the statistical analysis of a global network.

Honolulu is at the borderline. The problem is to account for $\delta a_{TT} = 1.03$ cm (100 yr)$^{-1}$ and $\delta h_{SL} = 12.7$ cm (100 yr)$^{-1}$ in response to ocean warming and freshening. "Steric" sea level due to variation of the underlying density field can be separated into warming and freshening components, according to

$$\begin{aligned}\delta h_{\text{STERIC}} &= -\int dz\ \delta\rho/\rho \\ &= -\int dz\ (\alpha\delta T - \beta\delta S) \\ &= \delta h_T + \delta h_S. \end{aligned} \tag{83}$$

Perturbations of the M_2 amplitude depend on the perturbation of the density field according to

$$\delta a_{TT} = -a_{IT}\lambda(\delta h_T + \delta h_S). \tag{84}$$

Changes in sea level are a sum of thermal expansion and eustatic rise. The eustatic rise can be estimated from δh_S depending on the source of the freshwater. Here a distinction is made between the melting of floating ice (with no attendant rise in sea level) and the melting of continental ice sheets. (However, δa_{TT} is independent of the source of freshening.) Writing $\delta h_S = \delta h_{S\ \text{sea}} + \delta h_{S\ \text{cont}}$, $r = \delta h_{S\ \text{cont}}/\delta h_S$, one can show that

$$\delta h_{SL} = \delta h_T + (\rho/\Delta\rho) r \delta h_S, \tag{85}$$

where $\Delta\rho/\rho = 28/1028$ is the fractional density difference of seawater over freshwater. The large multiplier $\rho/\Delta\rho = 36.7$ is derived from conservation of mass (Munk 2003). It arises because freshening depends on $\delta\rho/\Delta\rho$ and not on the steric ratio $\delta\rho/\rho$.

In each of the rows in Table 5 we have specified three values (in italics) to compute the remaining four values. Rows a–c correspond to the values for global freshening and heating from recent surveys by Antonov et al. (2002). Using $\delta h_S = 0.5$ cm cycle^{-1}, the total inferred melt volume is $\delta h_S(\rho/\Delta\rho)$(ocean area) = 600 km^3 yr^{-1} and is of the right magnitude (Wadhams 2000), but the uncertainties are so large that no clear choice can be made between row a (melting of sea ice) and row b (continental export). Sea level is very sensitive to this choice, and the Honolulu record would indicate contributions of comparable magnitude (row c). However, the inferred amplitude a_{TT} is only 0.5 times that observed.

Rows d–g of Table 5 take the Honolulu amplitudes and sea level as given. Row f with Levitus warming can be ruled out as it infers a sea ice melt volume an order of magnitude larger than measured. Rows d and e yield freshening far below the Antonov limits of 0.5 ± 0.2 cm

TABLE 5. Changes in amplitude and sea level [cm (100 yr)$^{-1}$]. For each row (a–g) four values are computed from three assumed values (italics). Right two columns are Honolulu amplitude and sea level changes according to Eqs. (84) and (85).

	$\delta h_{\mathrm{S\ cont}}$	$\delta h_{\mathrm{S\ sea}}$	δh_{S}	δh_{T}	δh_{ST}	δa_{TT}	δh_{SL}
(a)	*0*	0.5	*0.5*	*5*	5.5	0.45	5
(b)	0.5	*0*	*0.5*	*5*	5.5	0.45	23.4
(c)	0.21	0.29	*0.5*	*5*	5.5	0.45	*12.7*
(d)	*0*	−0.185	−0.185	12.7	12.5	*1.03*	*12.7*
(e)	0.0052	*0*	0.0052	12.5	12.5	*1.03*	*12.7*
(f)	0.210	7.31	7.52	*5*	12.5	*1.03*	*12.7*
(g)	0.019	0.48	*0.5*	12.0	12.5	*1.03*	*12.7*

(100 yr)$^{-1}$ (row d infers a freshwater transport *into* continents). This leaves row g with thermal expansion accounting for 12.0 out of 12.7 cm (100 yr)$^{-1}$ sea level rise, and the remainder due to continental input.

This surmise is based on many questionable assumptions: our zero correction for Honolulu ground motion may be seriously in error, the Levitus warming estimate may be too small, and the freshening estimate may not be significant; the venerable Honolulu record may be too short.

7. Conclusions

Observations in the last decade have shown that intensive scattering interactions over topography between surface and internal tide modes take place on a global scale. Accordingly, the energies are of comparable magnitude (as should have long been obvious from the known strong interference between baroclinic and barotropic tidal currents). This implies a small but measurable contribution to tidal "constants" by the surface manifestation of internal tides. The short and slow internal tides (relative to the surface tides) are severely modulated by low-frequency ocean variability.

The surface and internal components of the 1915–2000 Honolulu tide have been separated (to a point) from the composite record by a combined analysis in the frequency and Cartesian domains. Figure 18 is a pictorial summary of the Honolulu M_2 tidal amplitude (for those who can remember analog clock faces). The long surface tide hand points steadily at 1:00 P.M. (60° Greenwich epoch). The short internal tide hand has rotated during the twentieth century from a position near nine o'clock to 10:36. For shorter periods, from year to year, the short hand twirls all around the circle, making it difficult to determine its mean angle. The tide gauge is a composite clock with the short hand pivoted around the end of the long hand. The composite hand has lengthened (the recorded tide amplitude has increased) as the internal tide hand has turned from a neutral angle to a supporting angle.

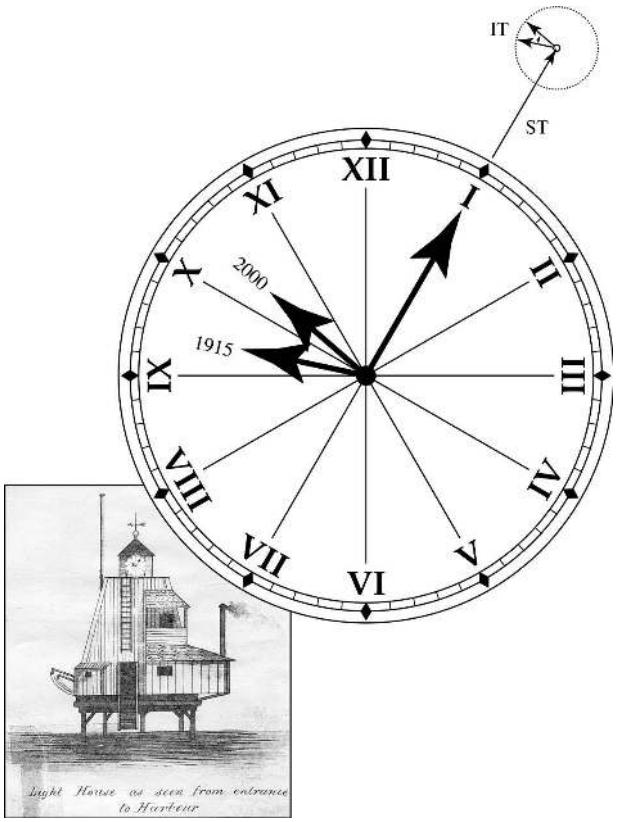

FIG. 18. The Honolulu tide clock. The twentieth-century recorded (surface plus internal) M_2 amplitude has increased by 1 cm as a result of a clockwise rotation of the mean internal tide vector.

In addition to the secular trend, there is a strong interannual variability that is coherent and in phase with the mean sea level (also extracted from the tide record): the composite M_2 amplitude is large when sea level is high. We attribute the interannual and secular variability to a modulation of the internal tide phase speed (and hence recorded phase angle) between the generation area and Honolulu harbor. Mean sea level is considered as a proxy for the variable density structure. The extraction of the two coherent time series (M_2 amplitude and mean sea level) from a century-long mid-ocean record can provide a unique framework for speculating on global sea level rise. The present analysis is severely hampered by the lack of understanding of the transition of internal waves from offshore to coastal waters. Ongoing geodetic measurements will provide improved estimates of the crucial corrections for ground motion. The relative contribution of sea ice melting to ocean freshening remains to be determined.

There has been no closure in the global budget; the relative contributions of thermal expansion and conti-

nental water export are still in doubt. Our interpretation of the Honolulu record somewhat favors warming over melting as the dominant contribution to twentieth-century sea level. However, the relative capacity of warming is inherently limited,[10] and it is dangerous to extrapolate twentieth-century sea level into the future.

Acknowledgments. We are grateful to Mark Merrifield, Peter Holloway, and Richard Ray for their advice and help. Author W. Munk holds the Secretary of the Navy Chair in Oceanography at the Scripps Institution of Oceanography.

APPENDIX A

Notation

In the following formulas

$$\alpha \equiv \overline{\theta^2} = -2\ln\nu. \tag{A1}$$

The frequency relative to the M_2 carrier frequency f_c is designated by

$$\beta = \frac{f - f_c}{f_\theta}, \quad \beta_j = \frac{jT^{-1}}{f_\theta} = \frac{2\pi j}{\tau}, \tag{A2}$$

where $j = 0, \pm 1, \ldots$ refers to the harmonics of record length T, f_θ is the characteristic frequency of phase modulation, and $\tau = 2\pi f_\theta T$.

We define the functions

$$F(\alpha, \beta) = 2\sum_{n=1}^{\infty} \frac{n\alpha^n}{n!(\beta^2 + n^2)}, \tag{A3}$$

$$G(\alpha, \beta, \tau) = 2\sum_{n=1}^{\infty} \left[\frac{n\alpha^n}{n!(\beta^2 + n^2)}\, q(\beta, \tau)\right], \tag{A4}$$

and

$$q(\beta, \tau) = 1 + \frac{\beta^2 - n^2}{\beta^2 + n^2}\frac{1 - e^{-n\tau}}{n\tau}\cos\beta\tau - \frac{2n\beta}{\beta^2 + n^2}\frac{e^{-n\tau}}{n\tau}\sin\beta\tau. \tag{A5}$$

[10] Present sea level *rates* of order 0.1 m (100 yr)$^{-1}$ compare to 1 m (100 yr)$^{-1}$ during the late Holocene; 5° warming of the upper 1000 m raises sea level by only 1 m; melting has the ultimate capacity for 100 m.

The associated "harmonic functions" are

$$F_j(\alpha) \equiv F(\alpha, \beta_j),$$
$$G_j(\alpha, \tau) \equiv G(\alpha, \beta_j, \tau), \quad \text{and}$$
$$q_j(\tau) = 1 + \frac{\beta_j^2 - n^2}{\beta_j^2 + n^2}\frac{1 - e^{n\tau}}{n\tau}, \tag{A6}$$

with the important special cases

$$F_0(\alpha) = 2\sum_{n=1}^{\infty}\frac{\alpha^n}{nn!}, q_0 = 1 - \frac{1 - e^{n\tau}}{n\tau} = \frac{1}{2}n\tau - \frac{1}{6}(n\tau)^2 + \cdots, \tag{A7}$$

and

$$G_0(\alpha, \tau) = 2\sum_{n=1}^{\infty}\left[\frac{\alpha^n}{nn!}\, q_0(\tau)\right] = \tau\left[-1 + e^{\alpha}\left(1 - \frac{1}{3}\alpha\tau\right) + \cdots\right]. \tag{A8}$$

The expansions in Eqs. (A7) and (A8) are for short record lengths, $\tau \to 0$. For long records

$$\tau \to \infty, \quad q \to 1, \quad G \to F, \quad \text{and} \tag{A9}$$

$$\sum_{j=-\infty}^{\infty} F_j(\alpha) = (-1 + \nu^{-2})\tau. \tag{A10}$$

It may be convenient to use the analytical representations

$$F(\alpha, \beta) = \Re[(-\alpha)^{i\beta}\Gamma(-i\beta) + (-\alpha)^{-i\beta}\Gamma(i\beta) + (i\beta^{-1}) - (-\alpha)^{i\beta}\Gamma(1 - i\beta, -\alpha) + (-\alpha)^{-i\beta}\Gamma(1 + i\beta, -\alpha)] \tag{A11}$$

and

$$F_0(\alpha) = 2\Re[-\gamma - \Gamma(0, \alpha) - \ln(-\alpha)] = 2\alpha + O\alpha^2, \tag{A12}$$

where $\gamma = 0.577$ is Euler's constant and $\Gamma(z) = \int_0^\infty t^{z-1}e^t\, dt$ is the Euler gamma function. Further,

$$G_0(\alpha, \tau) = 2\tau^{-1}\Re\{-\alpha\Phi(\mathbf{a}, \mathbf{b}, \alpha) + \alpha e^{-\tau}\Phi(\mathbf{a}, \mathbf{b}, \alpha e^{-\tau}) - \tau[\gamma + \Gamma(0, -\alpha) + \ln(-\alpha)]\}, \tag{A13}$$

where Φ is the generalized hypergeometric function with $\mathbf{a} = (1, 1, 1)$ and $\mathbf{b} = (2, 2, 2)$.

APPENDIX B

Evaluation of Spectral Integrals

The double integral in Eq. (19) is evaluated. Setting $\Delta t = t_1 - t_2$ and $y = 2\pi\Delta t f_\theta$ we get

$$\langle HH^* \rangle = \frac{\nu^2 a_{\mathrm{IT}}^2}{2}\left[\mathrm{sinc}^2(f_c - f)T + \frac{1}{T^2}\sum_{n=1}^{\infty}\frac{(\overline{\theta^2})^n}{n!}\int\int_{-T/2}^{T/2} dt_1\, dt_2\, e^{-2\pi i(f-f_c)\Delta t - 2\pi n f_\theta|\Delta t|}\right]$$

$$= \frac{\nu^2 a_{\mathrm{IT}}^2}{2}\left[\mathrm{sinc}^2(f_c - f)T + \frac{1}{2\pi f_\theta T^2}\sum_{n=1}^{\infty}\frac{(\overline{\theta^2})^n}{n!}\int_{-T/2}^{T/2} dt \int_{-(T/2+t)2\pi f_\theta}^{(T/2-t)2\pi f_\theta} dy\, e^{-n|y|}e^{-i\beta y}\right]. \quad \text{(B1)}$$

The second term in brackets can be written

$$\frac{G(\overline{\theta^2},\beta,\tau)}{\tau} \equiv \frac{1}{\tau}\sum_{n=1}^{\infty}\frac{(\overline{\theta^2})^n}{n!}\frac{1}{T}\int_{-T/2}^{T/2} dt\left[\int_{-(T/2+t)2\pi f_\theta}^{(T/2-t)2\pi f_\theta} dy\, e^{-n|y|}e^{-i\beta y}\right]$$

$$= \frac{1}{\tau}\sum_{n=1}^{\infty}\frac{(\overline{\theta^2})^n}{n!}\frac{1}{T}\int_{-T/2}^{T/2} dt\left[\int_{-(T/2+t)2\pi f_\theta}^{0} dy\, e^{(n-i\beta)y} + \int_{0}^{(T/2-t)2\pi f_\theta} dy\, e^{-(n+i\beta)y}\right]$$

$$= \frac{2}{\tau}\sum_{n=1}^{\infty}\frac{(\overline{\theta^2})^n}{n!}\frac{n}{(n^2+\beta^2)}\left\{1 + \frac{\beta^2 - n^2}{\beta^2 + n^2}\left[\frac{1 - e^{-n\tau}\cos(\tau\beta)}{n\tau}\right] - \frac{2n\beta}{n^2+\beta^2}\frac{e^{-n\tau}}{n\tau}\sin(\tau\beta)\right\}, \quad \text{(B2)}$$

where $\tau = 2\pi f_\theta T$ and $\beta = (f - f_c)/f_\theta$.

APPENDIX C

Amplitude Modulation

The sea surface height model, h, is of the form

$$h(t) = [a_{\mathrm{IT}} + \delta a_{\mathrm{IT}}(t)]e^{i[2\pi f_c t - \theta(t)]}, \quad \text{(C1)}$$

where f_c is the tide frequency, a_{IT} is the mean amplitude, and θ and $\delta a_{\mathrm{IT}}(t)$ are the statistical, internal tide phase and amplitude variations. Both $\theta(t)$ and $\delta a_{\mathrm{IT}}(t)$ are assumed to have a zero mean and Lorentzian power spectrum for the forms

$$S_\theta = \frac{\overline{\theta^2}}{\pi}\frac{f_\theta}{f^2 + f_\theta^2} \quad \text{and} \quad S_{\delta a_{\mathrm{IT}}} = \frac{\langle \delta a_{\mathrm{IT}}^2 \rangle}{\pi}\frac{f_a}{f^2 + f_a^2}. \quad \text{(C2)}$$

The spectra are normalized such that the variances of θ and δa_{IT} are $\overline{\theta^2}$ and $\langle \delta a_{\mathrm{IT}}^2 \rangle$. As before, the phase structure function, D, is

$$D(|\Delta t|) = \langle [\theta(t_1) - \theta(t_2)]^2 \rangle = 2\overline{\theta^2}(1 - e^{-2\pi f_\theta|\Delta t|}), \quad \text{(C3)}$$

and similarly the amplitude correlation function is given by

$$\langle \delta a_{\mathrm{IT}}(t_1)\delta a_{\mathrm{IT}}(t_2) \rangle = \langle \delta a_{\mathrm{IT}}^2 \rangle e^{-2\pi f_a|\Delta t|}. \quad \text{(C4)}$$

The Fourier transform of Eq. (C1) is

$$H(\omega) = \frac{a_{\mathrm{IT}}}{\sqrt{2}T}\int_{-T/2}^{T/2} e^{2\pi i(f_c - f)t}e^{-i\theta(t)}\, dt + \frac{1}{\sqrt{2}}\int_{-T/2}^{T/2} \delta a_{\mathrm{IT}}(t)e^{2\pi i(f_c - f)t}e^{-i\theta(t)}\, dt, \quad \text{(C5)}$$

and the spectral power is computed by multiplying Eq. (C5) by its complex conjugate, taking the expected value, and assuming $\langle \delta a_{\mathrm{IT}}\theta \rangle = 0$, which yields

$$\langle HH^* \rangle = \frac{a_{\mathrm{IT}}^2}{2T^2}\int\int_{-T/2}^{T/2} dt_1\, dt_2 \times \left[1 + \frac{\langle \delta a_{\mathrm{IT}}(t_1)\delta a_{\mathrm{IT}}(t_2) \rangle}{a_{\mathrm{IT}}^2}\right]e^{-2\pi i(f - f_c)\Delta t}e^{-D(|\Delta t|)/2}. \quad \text{(C6)}$$

The first term ($\delta a_{\mathrm{IT}} = 0$) is identified with pure phase modulation and is the previously derived Eq. (16). We call this term $\langle HH^* \rangle_{\mathrm{phase}}$. The integral of the second term is a combination of phase and amplitude modulation effects and can be evaluated with the help of Eq. (C4), writing

$$\frac{\langle \delta a_{\mathrm{IT}}(t_1)\delta a_{\mathrm{IT}}(t_2) \rangle}{a_{\mathrm{IT}}^2}e^{-(1/2)D(|\Delta t|)} = \epsilon^2\nu^2 e^{-2\pi f_a|\Delta t|}\exp(\overline{\theta^2})e^{-2\pi f_\theta|\Delta t|} \quad \text{(C7)}$$

$$= \epsilon^2\nu^2\left[\sum_{n=0}^{\infty}\frac{(\overline{\theta^2})^n}{n!}e^{-2\pi(f_a + nf_\theta)|\Delta t|}\right], \quad \text{(C8)}$$

where $\epsilon^2 = \langle \delta a_{\rm IT}^2 \rangle / a_{\rm IT}^2$ and $\Delta t = t_1 - t_2$. Proceeding as previously (appendix B),

$$\langle HH^* \rangle_{\rm amp} = \frac{a_{\rm IT}^2 \nu^2 \epsilon^2}{2} \sum_{n=0}^{\infty} \frac{(\overline{\theta^2})^n}{n!} \frac{2}{\tau_n} \frac{1}{(1+\beta_n^2)} \times \left(1 + \frac{\beta_n^2 - 1}{\beta_n^2 + 1} \frac{1 - e^{-\tau_n}}{\tau_n} \right), \quad \text{(C9)}$$

where $\beta_n = (f - f_c)/(f_a + n f_\theta)$, $\tau_n = \tau_a + n\tau$, and $\tau_a = 2\pi f_a T$. Note that the summation in Eq. (C9) starts at $n = 0$; this means that there is no contribution to $E^{\rm LINE}$. In the limit of no phase variance (i.e., $\overline{\theta^2} \to 0$) it is found that the $\langle HH^* \rangle_{\rm phase}$ reduces to $\delta(j) a_{\rm IT}^2/2$ and $\langle HH^* \rangle_{\rm amp}$ is simply the assumed (Lorentzian) spectrum.

APPENDIX D

Parameter Estimates in Table 1

Sampling errors of the Cartesian parameters in section 5a are

$$\delta\langle X \rangle = \pm(\sigma_X^2/N)^{1/2}, \quad \langle Y \rangle = \pm(\sigma_Y^2/N)^{1/2}, \quad \langle X^2 \rangle = \pm 2(\sigma_X^2 \langle X^2 \rangle/N)^{1/2},$$
$$\langle Y^2 \rangle = \pm 2(\sigma_Y^2 \langle Y^2 \rangle/N)^{1/2}, \quad \text{and} \quad \langle XY \rangle = \pm(\sigma_X^2 \langle Y^2 \rangle/N + \sigma_Y^2 \langle X^2 \rangle/N)^{1/2}. \quad \text{(D1)}$$

The number N of independent samples in the time series is estimated using the temporal correlation functions of X and Y, which show decorrelation to values less than 0.5 at roughly 3-month lag, yielding the 95% confidence limits

$$\delta A = \pm 1.96(\sigma_x^4/2N + \sigma_y^4/2N)^{1/2}, \quad B = \pm 1.96(\sigma_x^2 \sigma_y^2/N)^{1/2}, \quad \delta C = \pm 1.96(\sigma_x^2/N)^{1/2}, \quad \text{and} \quad \delta D = \pm 1.96(\sigma_y^2/N)^{1/2}. \quad \text{(D2)}$$

Parameter and error estimates for $a_{\rm IT}$, $a_{\rm ST}$, $\theta_{\rm IT}$, $\theta_{\rm ST}$, and ν are obtained by considering an expanded group of the auxilliary observables associated with A, $A \pm \delta A$, B, $B \pm \delta B$, C, $C \pm \delta C$, and D, $D \pm \delta D$, which form 81 possible combinations (e.g., one combination is A, $B + \delta B$, $C - \delta C$, D). For each of the 81 sets of the auxilliary observables the objective function $J^2(\nu)$ is computed and $J^2_{\rm min}$ identified. The parameter set with the smallest $J^2_{\rm min}$ is considered the best estimate of $a_{\rm IT}$, $a_{\rm ST}$, $\theta_{\rm IT}$, $\theta_{\rm ST}$, and ν (Fig. D1). Errors are computed from the max/min deviations of the parameter over the 81 cases. These estimates assume that σ_x^2 and σ_y^2 are known exactly. Last, the parameter f_θ is estimated by fitting a Lorentzian to the spectrum of the unwrapped internal tide phase [Eq. (63)].

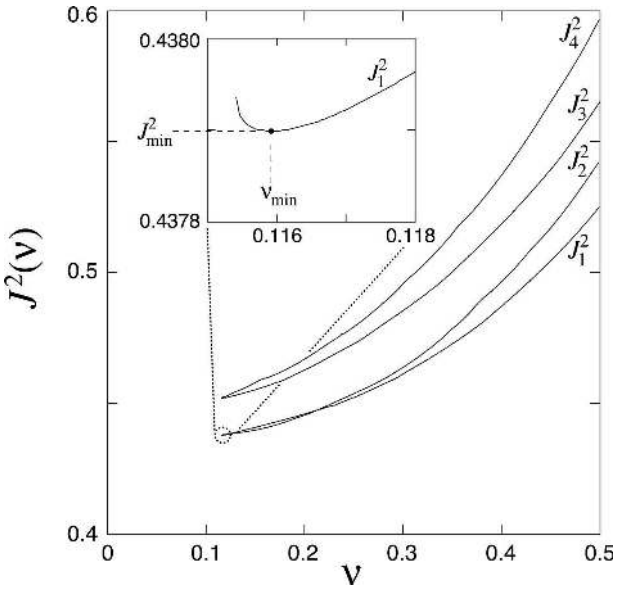

FIG. D1. The "cost function" $J^2(\nu)$ for the Honolulu demodulates. Four of the five $\theta_{\rm IT}$ solutions are independent, yielding four branches of $J^2(\nu)$. Inset shows an enlargement near $J^2_{\rm min}$. The figure is one of 81 such plots, giving the lowest $J^2_{\rm min}$.

In generating $X(t)$ and $Y(t)$ we have chosen a demodulation window $T \sim 1/6$ yr, thus limiting the frequency window to $f_c \pm f_L$, $f_L = 1/(2T) = 3.33$ cpy. This avoids the N_2 overlap at the expense of containing only a fraction of the band energy and the phase variance.

To examine the resolution limitations, a truncated Lorentzian phase spectrum of the form

$$S_\theta(f) = \begin{cases} \dfrac{\overline{\theta^2}}{2\tan^{-1}(f_L/f_\theta)} \dfrac{f_\theta}{f^2 + f_\theta^2} & -f_L \le f \le f_L \\ 0 & |f| > f_L \end{cases} \quad \text{(D3)}$$

is used to generate the toy model random phases. The spectrum is normalized so that

$$\int_{-\infty}^{\infty} S_\theta(f)\, df = \overline{\theta^2}. \tag{D4}$$

The Cartesian analysis yields values much closer to the assumed values for $f_L = 3.34$ cpy than for $f_L = \infty$ (Table 1, rows b and d).

To correct the $f_L = \infty$ estimates for $\overline{\theta^2}$, $a_{\rm IT}$, and $E^{\rm BAND}$, we adopt the following procedure. The phase variance is corrected using the Lorentzian formula,

$$\overline{\theta^2}_c = \overline{\theta^2}\,\frac{\pi}{2\tan^{-1}(f_L/f_\theta)}. \tag{D5}$$

The corrected band energy is $(E^{\rm BAND})_c = RE^{\rm BAND}$, $R = 1.71/1.33 = 1.29$ (from Table 1, rows b and d). Last,

$$a_{\rm IT} = \left[\frac{2(E^{\rm BAND})_c}{1-\nu_c^2}\right]^{1/2}. \tag{D6}$$

APPENDIX E

Surface Displacements of Baroclinic Waves

A rigid seafloor and free surface at the air–water interface impose boundary conditions[E1]:

$$\zeta(x, y, -D, t) = 0 \quad \text{and} \quad \zeta(x, y, 0, t) = \frac{p(x, y, 0, t)}{\rho_0 g}. \tag{E1}$$

We distinguish between the offshore depth $D_{\rm RO}$ for the propagation of the long Rossby waves and $D_{\rm IT} < D_{\rm RO}$ for the propagation of the internal tides in the coastal waveguide. For linear internal and Rossby waves the upper condition expressed in terms of ζ only becomes

$$\frac{d\zeta_{\rm IW}}{dz} - \frac{gk_h^2}{\omega^2 - f^2}\,\zeta_{\rm IW} = 0 \quad \text{and} \quad \frac{d\zeta_{\rm RO}}{dz} + \frac{g\lambda^2}{f^2}\,\zeta_{\rm RO} = 0, \tag{E2}$$

where f is the Coriolis parameter, g is the acceleration due to gravity, k_h is the magnitude of the horizontal wavenumber, and $\lambda^2 = -(k_h^2 + \beta k_x/\omega)$ (Pedlosky 1987, p. 379).[E2] The phase speed of the internal tide $c_{\rm IT}$ is modulated by long Rossby waves of the form $\exp i(k_x x + k_y y - \omega t)$ (x is positive eastward) with surface displacement $\zeta_{\rm RO}$. The *modulated* internal tide and *modulating* Rossby wave have vertical modal structure governed by the wave equations

$$\frac{d^2\zeta_{\rm IW}}{dz^2} + k_h^2\,\frac{N^2(z) - \omega^2}{\omega^2 - f^2}\,\zeta_{\rm IW} = 0 \quad \text{and} \quad \frac{d^2\zeta_{\rm RO}}{dz^2} + \lambda^2\,\frac{N^2(z)}{f^2}\,\zeta_{\rm RO} = 0 \tag{E3}$$

subject to the boundary conditions in Eqs. (E1) and (E2). For a buoyancy frequency $N = N_0$ (a constant), internal and Rossby waves have vertical modes of the form $\zeta = A\sin[m(z + D)]$. The vertical wavenumber m for mode j follows the relation

$$Dm = \pi j + \epsilon + O(\epsilon^2), \tag{E4}$$

with

$$\epsilon_{\rm IW} \simeq \frac{D}{\pi j g}(N_0^2 - \omega^2)\,\frac{1}{j\pi}\,\frac{\Delta\rho}{\rho} \quad \text{and} \quad \epsilon_{\rm RO}\,\frac{D}{\pi j g}N_0^2 = \frac{1}{j\pi}\,\frac{\Delta\rho}{\rho}, \tag{E5}$$

where $\Delta\rho$ is the difference in density across the whole water column. In either case the surface expression of the wave is

$$\zeta(z = 0) = A\sin(mD) = A\sin(\epsilon)\cos(\pi j). \tag{E6}$$

For mode $j = 1$, the surface and internal amplitudes are related by[E3]

$$\zeta_0 \equiv \zeta(z = 0) = -A\pi^{-1}\Delta\rho/\rho. \tag{E7}$$

The first-order solution to Eq. (E3) consistent with Eqs. (E4) and (E5) is

$$\zeta_{\rm RO} = \zeta_0\,\frac{\pi g}{DN_0^2}\sin\frac{\pi z}{D}, \tag{E8}$$

with a resulting density perturbation

$$\delta\rho = (d\rho/dz)\zeta_{\rm RO} = (-\rho_0 N_0^2 g^{-1})\zeta_{\rm RO}, \tag{E9}$$

[E1] The condition at $z = 0$ is a linearization of the condition $p(x, y, z = \zeta) = 0$ with vertical velocity equal to $d\zeta/dt$. The analysis is simplified further by imposing the "rigid lid" at the surface boundary, $\zeta(x, y, 0, t) = 0$ with the surface displacement subsequently determined by Eq. (E1).

[E2] The eigenvalues, λ^2, are all positive, and the Rossby internal deformation radius is $1/\lambda$. The minus sign in the definition of λ^2 imposes westward phase propagation.

[E3] For the two-layer case Eq. (70) the relation is $\zeta_0/A = -\Delta\rho/\rho$ and of similar form as $-(j\pi)^{-1}\,\Delta\rho/\rho$ for continuously statified internal waves and Rossby waves, but the associated bottom pressures are very different. For continuously stratified internal waves the bottom pressure $p(-D) = \rho_0\int_{-D}^{0}(N^2 - \omega^2)\zeta_{\rm IW}\,dz$ remains finite in the limit of low frequencies, of order ϵ (ϵ^3) for odd (even) modes; for odd modes, $p(-D) = -2\rho g\zeta_0$ has 2 times the amplitude of pressure just beneath the surface. For the two-layer case and for Rossby waves, $p(-D) = -\rho_0\int_{-D}^{0}\omega^2\zeta_{\rm IW/RO}\,dz$ vanishes in the low-frequency limit.

which leads to

$$\delta N^2(z) = (g/\rho)d(\delta\rho)/dz = -\zeta_0 \frac{\pi^2 g}{D_{\mathrm{RO}}^2} \cos\left(\frac{\pi z}{D_{\mathrm{RO}}}\right). \tag{E10}$$

Next the perturbation to the internal tide by the Rossby wave perturbed density structure is computed. Perturbation theory (Gasiorowicz 1974, chapter 16), gives the first-order correction to the internal wave wavenumber and thus the fractional phase speed change:

$$\frac{\delta C_p}{C_p} = -\frac{1}{2}\frac{\delta k_n^2}{k_n^2} = \frac{1}{2}\int_0^D \left[\frac{N^2(z) - f^2}{N^2(z) - \omega^2}\right] \delta N^2(z) W_n^2(z)\, dz, \tag{E11}$$

where k_n^2 is the unperturbed wavenumber and $W_n(z)$ is the unperturbed mode function, normalized such that $\int_0^D (N^2 - f^2) W_n W_m\, dz = \delta_{nm}$. The internal tide mode-1 function is

$$W_{\mathrm{IT}}(z) = \left[\frac{2}{D_{\mathrm{IT}}(N_0^2 - f^2)}\right]^{1/2} \sin\left(\frac{\pi z}{D_{\mathrm{RO}}}\right), \tag{E12}$$

and substituting Eqs. (E10) and (E12) into Eq. (E11) and integrating yields

$$\frac{\delta C_{\mathrm{IT}}}{C_{\mathrm{IT}}} = \frac{\pi^2}{2}\frac{\mathrm{sinc}(n)}{1 - n^2/4}\frac{g\zeta_0}{(N_0^2 - \omega^2)D_{\mathrm{RO}}^2} \simeq \frac{\pi^2}{2}\frac{\mathrm{sinc}(n)}{1 - n^2/4}\frac{\zeta_0/D_{\mathrm{RO}}}{\Delta\rho/\rho}, \tag{E13}$$

where $n = D_{\mathrm{IT}}/D_{\mathrm{RO}}$ and $\mathrm{sinc}\ n = \sin(\pi n)/\pi n$.

REFERENCES

Agnew, D. C., 1986: Detailed analysis of tide gauge data: A case history. *Mar. Geodesy,* **10,** 231–255.

Alford, M. H., M. C. Gregg, and M. A. Merrifield, 2006: Structure, propagation, and mixing of energetic baroclinic tides in Mamala Bay, Oahu, Hawaii. *J. Phys. Oceanogr.,* **36,** 997–1018.

Antonov, J. I., S. Levitus, and T. P. Boyer, 2002: Steric sea level variations during 1957–1994: Importance of salinity. *J. Geophys. Res.,* **107,** 8013, doi:10.1029/2001JC000964.

Caccamise, D. J., II, M. A. Merrifield, M. Bevis, J. Foster, Y. L. Firing, M. S. Schenewerk, F. W. Taylor, and D. A. Thomas, 2005: Sea level rise at Honolulu and Hilo Hawaii: GPS estimates of differential land motion. *Geophys. Res. Lett.,* **32,** L03607, doi:10.1029/2004GL021380.

Cartwright, D. E., 1972: Secular changes in the oceanic tide at Brest, 1711–1936. *Geophys. J. Roy. Astr. Soc.,* **30,** 433–449.

Chiswell, S. M., 2002: Energy levels, phase and amplitude modulation of the baroclinic tide off Hawaii. *J. Phys. Oceanogr.,* **32,** 2640–2651.

Colosi, J. A., R. C. Beardsley, J. F. Lynch, G. Gawarkiewicz, C. S. Chiu, and A. Scotti, 2001: Observations of nonlinear internal waves on the outer New England continental shelf during the summer Shelfbreak Primer study. *J. Geophys. Res.,* **106,** 9587–9601.

Defant, A., 1932: Die Gezeiten und inneren Gezeitenwellen des Atlantischen Ozeans (The tides and inner tidal currents of the Atlantic Ocean). Deutsch Atlantische Expend. Meteor. 1925–1927, Wiss. Erg., Bd. 7, Heft 1, 318 pp.

Dushaw, B. D., B. D. Cornuelle, P. F. Worcester, B. M. Howe, and D. S. Luther, 1995: Barotropic and baroclinic tides in the central North Pacific Ocean determined from long-range reciprocal acoustic transmissions. *J. Phys. Oceanogr.,* **25,** 631–647.

Ekman, V. W., and B. Helland-Hansen, 1931: Measurements of ocean currents (Experiments in the North Atlantic). Kungl. Fysiografisca Sallskapet i Lund Forhandlingar, Vol. 1, No. 1.

Flick, R. E., J. F. Murray, and L. C. Ewing, 2003: Trends in the U.S. Tidal Datum Statistics and Tide Range. *ASCE J. Waterway, Port, Coast. Ocean Eng.,* **129** (4), 155–164.

Gasiorowicz, S., 1974: *Quantum Physics.* John Wiley and Sons, 470 pp.

Gill, A. E., 1982: *Atmosphere–Ocean Dynamics.* Academic Press, 662 pp.

Grigg, R. W., and A. T. Jones, 1997: Uplift caused by lithospheric flexure in the Hawiian archipelego as revealed by elevated coral deposits. *Mar. Geol.,* **141,** 11–25.

Levitus, S., J. I. Antonov, T. P. Boyer, and C. Stephens, 2000: Warming of the World Ocean. *Science,* **287,** 2225–2229.

——, ——, J. Wang, T. L. Delworth, K. W. Dixon, and A. J. Broccoli, 2001: Anthropogenic warming of Earth's climate system. *Science,* **292,** 267–270.

Middleton, D., 1960: *An Introdution to Statistical Communication Theory.* McGraw-Hill, 1140 pp.

Mitchum, G. T., and S. M. Chiswell, 2000: Coherence of internal tide variations along the Hawaiian Ridge. *J. Geophys. Res.,* **105,** 653–661.

Moore, J. G., 1970: Relationship between subsidence and volcanic load, Hawaii. *Bull. Volcanol.,* **34,** 562–576.

——, and D. J. Fornari, 1984: Drowned reefs as indicators of the rate of subsidence of the island of Hawaii. *J. Geol.,* **92,** 752–759.

——, and D. A. Clague, 1992: Volcano growth and evolution of the island of Hawaii. *Geol. Soc. Amer. Bull.,* **104,** 1471–1478.

——, B. L. Ingram, K. R. Ludwig, and D. A. Clague, 1996: Coral ages and island subsidence; Hilo drill hole. *J. Geophys. Res.,* **101,** 11 599–11 605.

Munk, W., 2003: Ocean freshening, sea level rising. *Science,* **300,** 2041–2043.

——, and E. C. Bullard, 1963: Patching the long-wave spectrum across the tides. *J. Geophys. Res.,* **68,** 3627–3634.

——, and D. E. Cartwright, 1966: Tidal spectroscopy and prediction. *Philos. Trans. Roy. Soc. London,* **259,** 533–581.

——, and C. Wunsch, 1998: Abyssal recipes II: Energetics of tidal and wind mixing. *Deep-Sea Res. I,* **45,** 1977–2010.

——, B. Zetler, and G. W. Groves, 1965: Tidal cusps. *Geophys. J.,* **10,** 211–219.

Pedlosky, J., 1987: *Geophysical Fluid Dynamics.* Springer-Verlag, 710 pp.

Ray, R. D., and G. T. Mitchum, 1996: Surface manifestation of internal tides generated near Hawaii. *Geophys. Res. Lett.,* **23,** 2101–2104.

——, and ——, 1997: Surface manifestation of internal tides in the

deep ocean. *Progress in Oceanography,* Vol. 40, Pergamon, 135–162.

——, and D. E. Cartwright, 2001: Estimates of internal tide energy fluxes from TOPEX/Poseidon altimetry: Central North Pacific. *Geophys. Res. Lett.,* **28,** 1259–1262.

Rubin, K., C. H. Fletcher III, and C. Sherman, 2000: Fossiliferous Lana'I deposits formed by multiple events rather than a single giant tsunami. *Nature,* **408,** 675–681.

Schmitt, R. G., and D. C. Cox, 1992: Hawaiian Time. *Hawaiian J. Hist.,* **26,** 207–225.

Sverdrup, H. U., M. W. Johnson, and R. H. Fleming, 1942: *The Oceans: Their Physics, Chemistry and General Biology.* Prentice Hall, 1087 pp.

Wadhams, P., 2000: *Ice in the Ocean.* Gordon and Breach, 351 pp.

Watts, A. B., and U. S. ten Brink, 1989: Crustal structure flexure, and subsidence history of the Hawaiian Islands. *J. Geophys. Res.,* **94,** 10 473–10 500.

Zhong, S., and A. B. Watts, 2002: Constraints on the dynamics of mantle plumes from uplift of the Hawaiian Islands. *Earth Planet. Sci. Lett.,* **203,** 105–116.